Biointerface Research in Applied Chemistry
Platinum Open Access Journal (ISSN: 2069-5837)

Article
Volume 11, Issue 4, 2021, 11833 - 11855
https://doi.org/10.33263/BRIAC114.1183311855

Molecular Structure, Vibrational Spectral Investigations (FT-IR and FT-Raman), NLO, NBO, HOMO-LUMO, MEP Analysis of (E)-2-(3-pentyl-2,6-diphenylpiperidin-4-ylidene)-N-phenylhydrazinecarbothioamide Based on DFT and Molecular Docking Studies

Savithiri Sambandam [1,*], Bharanidharan Sarangapani [2], Sugumar Paramasivam [3], Rajeevgandhi Chinnaiyan [4]

[1] Department of Chemistry, Karpagam Academy of Higher Education, Coimbatore – 641 021, India; savithiri.chem@gmail.com (S.S.);
[2] Department of Physics, PRIST University, Puducherry – 605 007, India; bharani.dharan0@gmail.com (B.S.);
[3] Department of Physics, Dhaanish Ahmed College of Engineering, Tambaram, Chennai – 601 301, Tamilnadu, India; sugumar17283@gmail.com (S.P.);
[4] Department of Physics, Annamalai University, Annamalainagar – 608 002, Tamilnadu, India; rajeevphdphy@gmail.com (R.C.);
* Correspondence: savithiri.chem@gmail.com;

Scopus Author ID 56294087000
Received: 5.11.2020; Revised: 12.12.2020; Accepted: 16.12.2020; Published: 18.12.2020

Abstract: The molecular spectroscopic investigations of (*E*)-2-(3-pentyl-2,6-diphenylpiperidin-4-ylidene)-*N*-phenylhydrazine carbothioamide (3-PDPPPHC) are studied. The FT-IR and FT-Raman experimental spectra of the molecule have been recorded in the range of 4000–400 cm^{-1} and 4000–50 $cm^{-1,}$ respectively. The molecular structure, fundamental vibrational frequencies, and intensities of the vibrational bands were interpreted to aid structure optimizations based on the density functional theory (DFT) method with B3LYP/6-311++G(d,p) level of basis set. The complete vibrational assignments of wavenumbers were made based on total energy distribution (TED). The calculations' results were applied to the title compound's simulated spectra, which show good agreement with observed spectra. The dipole moment, polarizability, and first hyperpolarizability values were also computed. The stability of the molecule analyzing from hyper-conjugative interaction and charge delocalization of the title compounds were studied by NBO analysis. Frontier molecular orbitals (FMOs), molecular electrostatic potential (MEP), and thermodynamic properties were performed. Mulliken charges of the title molecule were also calculated and interpreted. The thermodynamic properties such as heat capacity, entropy, and enthalpy of the title compound were calculated at different gas-phase temperatures. To establish information about the interactions between protein and this novel compound theoretically, docking studies were carried out in detail.

Keywords: FT-IR; FT-Raman; NLO; NBO; FMO;molecular docking.

1. Introduction

Nitrogen-containing heterocyclic compounds, especially piperidones, gain considerable importance owing to their varied biological properties. Thiosemicarbazones show very interesting and important biological activity in pharmaceutical and industrial aspects as antibacterial [1], antifungal [2], antimalarial [3,4] antioxidant activity [5,6] anticancer [7-9]

and anticonvulsant [10] antimycobacterial activity [11], antiproliferative activity [12,13], Toxicity [14], cytotoxicity [15] and several biological activity of thiosemicarbazones [16-21]. However, little is known about piperidine-4-ones substituted with a thiosemicarbazone moiety possessing potential pharmacological activities such as antiviral and antiprotozoal activities [22-25]. A few semicarbazones, just as their sulfur analogs and their derivatives, have proved their efficiency and efficacy in combating various diseases [26]. Theoretical investigations of thiosemicarbazones were reported by DFT method [27-29]. NLO materials play a vital role in various fields such as fiber optics communications and optical signal processing. In the last two decades, intensive research has shown that organic crystals also exhibit non-linear optical efficiencies of greater magnitude than inorganic materials. Semicarbazones and thiosemicarbazone of substituted heterocyclic organic compounds, ketones, and acetophenones were accounted for to be potential organic NLO [30–32] materials. The FT-IR and FT-Raman spectra joined with quantum chemical computations have been recently used as an effective tool in the vibrational analysis of drug molecules [33], biological compounds [34] and natural products [35], since FT-Raman spectra and processed outcomes can help unambiguous distinguishing proof of the vibrational modes as well as the bonding and structural features of organic molecular systems. Both the IR and Raman spectroscopic investigations have been used to obtain the structural information on molecules. The present study aimed to investigate the molecular structural properties, vibrational and energetic data of 3-PDPPPHC, in the gas phase, due to its pharmaceutical importance. The ground and the excited state properties of the title molecule are B3LYP/6-311++G(d,p) hybrid functional is used for density functional theory (DFT) calculation. As vibrational and electronic spectroscopic studies provide very useful information about the structure and conformation of the molecules if utilized in collaboration with quantum chemical calculations, to obtain a complete description of molecular dynamics, vibrational wavenumber calculation, and the normal mode analysis has been administered at the DFT theory. The investigation of geometry, dipole moment, polarizability, first static hyperpolarizability, along with the molecular electrostatic potential surface will lead to a better understanding of the structural and spectral characteristics of the compound chosen for the study.

2. Materials and Methods

2.1. Experimental details.

2.1.1. Synthesis procedure.

(E)-2-(3-pentyl-2,6-diphenylpiperidin-4-ylidene)-N-phenylhydrazinecarbothioamide was synthesized by subsequent the procedure described in the literature [36]. The spectral data are reliable with the reported values [36].

2.1.2. FT-IR and FT-Raman spectra details.

The FT-IR spectrum of the synthesized 3-PDPPPHC was measured in the range 4000–400 cm^{-1} in AVATAR-330 FT-IR spectrometer (Thermo Nicolet) using KBr (pellet form) in the Department of Chemistry, Annamalai University, Chidambaram, Tamilnadu. FT-Raman spectrum was observed using laser source Nd:YAG 1064 nm as excitation wavelength in the region 4000-50 cm^{-1} on Bruker IFS 66v spectrophotometer equipped with an FRA 106 FT-

Raman module accessory and at a spectral resolution of 4 cm^{-1}. The FT-Raman spectrum was recorded at SAIF Laboratory, IIT Madras.

*2.2. Computational details***.**

2.2.1. DFT Calculation.

The DFT method performed the entire quantum chemical calculations using the Gaussian 09W program package [37]. The optimized structural bond parameters and fundamental vibrational frequencies were calculated. The vibrational frequency assignments were made with a high degree of accuracy. The TED analysis was made using the VEDA4 program [38]. The NBO calculations were performed using NBO 3.1 program [39] as implemented in the Gaussian 09W [37] package. The DOS spectrum was drawn with the help of the Gauss sum 3.0 program [40]. In the present work, the DFT approach with 6-311++G(d,p) as a basis for computation of molecular structure, vibrational frequencies, and energies of optimized structures was utilized. The Bond parameters, NLO, NBO, HOMO-LUMO, Mulliken atomic charges, MEP, and thermodynamic parameters were calculated using the B3LYP/6-311++G(d,p) basis set.

2.2.2. Molecular docking.

Metallo-β-lactamases (MBLs) one of the most significant and boundless components of protection from β-lactam anti-microbials, against which no clinically helpful inhibitors are as of now accessible. We report thus a structure-based high-throughput docking (HTD) crusade on clinically-applicable procured MBLs.

The study's objective is to demonstrate that piperidone derivatives bind to beta-lactamase enzymes and evaluate whether these molecules can be used as a potential drug. The structural information and the data for the target were collected from the “Protein Data Bank” (PDB). The PDB ID: 1EVE [41] was used as the template for our studies. They were predicting the most likely conformation of how a ligand will bind to a macromolecule and some relevant residues of the protein considered flexible during the docking simulation. Basic potential parameters fit protein-ligand binding, and data scoring functions are comparable with new hydrogen bonding term and new charge schemes.

Docking calculations were carried out on the Beta-lactamase enzyme protein model [42]. Essential hydrogen atoms, Kollman united atom type charges, and solvation parameters were added with AutoDock tools' aid [43].

3. Results and Discussion

3.1. Geometrical parameters.

The optimized molecular structure of 3-PDPPPHC with atom numbering scheme is shown in Fig. 1. The optimized structural parameters, such as bond lengths, bond angles, and dihedral angles, were determined at the DFT/B3LYP/6-311++G(d,p) basis set. The values are listed in Table 1. In this study, the C-C, C-N, C=S, N-H, and C-H bond distances are calculated and compared with structurally related molecules [44]. The calculated C-C bond distances in the heterocyclic ring are in the range of 1.573 – 1.518 Å, compared with the reported DFT value (1.585 – 1.508 Å) [44]. In addition, the DFT value of C-C bond lengths in phenyl also rings agreement with literature values [44]. The C=S bond length is calculated at 1.662 Å and

is also related to reported data 1.681 Å. The C-N bond lengths in the range 1.470 – 1.380 Å by the B3LYP method, respectively, are in agreement with the reported values 1.471 – 1.288 Å [44]. The optimized N-H bond lengths fall in the range 1.017 – 1.013 Å by B3LYP method with 6-311++G(d,p) basis set and comparing these values with literature value 1.000 – 0.993 Å, respectively. Also, the bond angles of C2-C1-N9 (107.96˚) and C4-C5-N9 (108.32˚), which are calculated at DFT/B3LYP/6-311++G(d,p) basis set and are form to decrease from 120˚. This is due to the phenyl group's substitution in connection with C1 and C5 carbon atoms in the piperidone ring. The piperidone ring essentially adopts chair conformation with all substituents equatorial as evident from the torsional angles N9–C1–C2–C3 = -58.88 and N9–C5–C4–C3 = 55.76 by B3LYP, respectively. In the optimized molecular structure, the thiosemicarbazone analog is nearly planar with the dihedral angle N26–N27–C32–N28 (176.62˚) adopts an *E*-configuration concerning the C3-N26 bond. The calculated values are comparable with reported values [44].

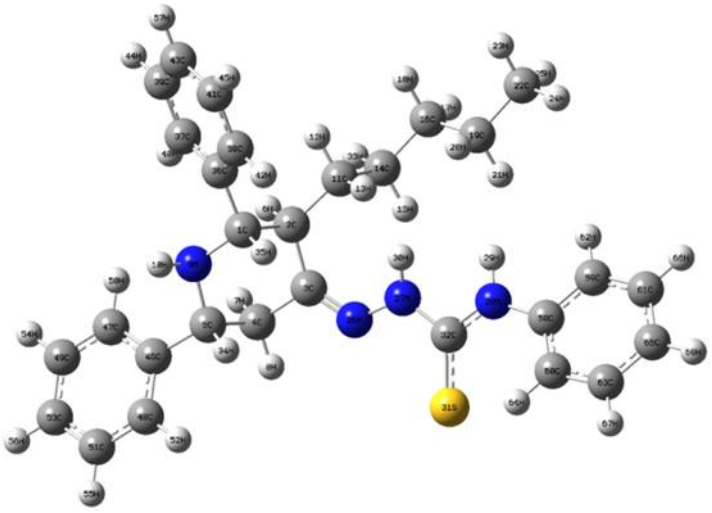

Figure 1. The optimized molecular structure of 3-PDPPPHC.

Table 1. The optimized bond parameters of 3-PDPPPHC.

Bond Lengths (Å)	DFT	Bond Angles (°)	DFT	Dihedral Angles (°)	DFT
C1-C2	1.573	C2-C1-N9	107.96	N9-C1-C2-C3	-58.8837
C1-N9	1.470	C2-C1-H35	106.62	N9-C1-C2-H6	51.5304
C2-C3	1.530	C2-C1-C36	113.40	N9-C1-C2-C11	166.6641
C2-C11	1.540	N9-C1-H35	112.05	H35-C1-C2-C3	61.6846
C3-C4	1.511	N9-C1-C36	109.02	H35-C1-C2-H6	172.0987
C3-N26	1.286	H35-C1-C36	107.84	H35-C1-C2-C11	-72.7675
C4-C5	1.551	C1-C2-C3	105.63	C36-C1-C2-C3	-179.791
C4-H7	1.097	C1-C2-H6	104.44	C36-C1-C2-H6	-69.3772
C4-H8	1.091	C1-C2-C11	114.25	C36-C1-C2-C11	45.7565
C5-N9	1.468	C3-C2-H6	104.96	C2-C1-N9-C5	61.2724
C5-H34	1.105	C3-C2-C11	120.28	C2-C1-N9-H10	-174.666
C5-C46	1.518	H6-C2-C11	105.82	H35-C1-N9-C5	-55.8321
N9-H10	1.017	C2-C3-C4	111.64	H35-C1-N9-H10	68.2296
C11-H12	1.095	C2-C3-N26	133.27	C36-C1-N9-C5	-175.125
C11-H13	1.100	C4-C3-N26	114.36	C36-C1-N9-H10	-51.0632
C11-C14	1.539	C3-C4-C5	108.36	C2-C1-C36-C37	72.8434
C14-H15	1.098	C3-C4-H7	111.30	C2-C1-C36-C38	-107.06
C14-C16	1.538	C3-C4-H8	109.66	N9-C1-C36-C37	-47.4609
C14-H33	1.098	C5-C4-H7	108.45	N9-C1-C36-C38	132.6359
C16-H17	1.098	C5-C4-H8	109.90	H35-C1-C36-C37	-169.34
C16-H18	1.099	H7-C4-H8	109.15	H35-C1-C36-C38	10.7569
C16-C19	1.536	C4-C5-N9	108.32	C1-C2-C3-C4	62.4067
C19-H20	1.099	C4-C5-H34	106.17	C1-C2-C3-N26	-107.045
C19-H21	1.100	C4-C5-C46	111.85	H6-C2-C3-C4	-47.6392

Bond Lengths (Å)	DFT	Bond Angles (°)	DFT	Dihedral Angles (°)	DFT
C19-C22	1.532	N9-C5-H34	111.58	H6-C2-C3-N26	142.9095
C22-H23	1.095	N9-C5-C46	110.79	C11-C2-C3-C4	-166.505
C22-H24	1.095	H34-C5-C46	108.07	C11-C2-C3-N26	24.0441
C22-H25	1.095	C1-N9-C5	115.41	C1-C2-C11-H12	-53.1277
N26-N27	1.359	C1-N9-H10	109.25	C1-C2-C11-H13	60.1182
N27-H30	1.013	C5-N9-H10	109.64	C1-C2-C11-C14	-172.12
N27-C32	1.388	C2-C11-H12	107.16	C3-C2-C11-H12	179.6308
N28-H29	1.013	C2-C11-H13	111.80	C3-C2-C11-H13	-67.1233
N28-C32	1.380	C2-C11-C14	113.46	C3-C2-C11-C14	60.6383
N28-C58	1.413	H12-C11-H13	103.92	H6-C2-C11-H12	61.1982
S31-C32	1.662	H12-C11-C14	107.90	H6-C2-C11-H13	174.444
S31-H64	2.683	H13-C11-C14	111.95	H6-C2-C11-C14	-57.7944
C36-C37	1.403	C11-C14-H15	110.84	C2-C3-C4-C5	-61.5417
C36-C38	1.400	C11-C14-H16	114.26	C2-C3-C4-H7	57.6231
C37-C39	1.394	C11-C14-H33	107.50	C2-C3-C4-H8	178.503
C38-C41	1.396	H15-C14-C16	109.44	N26-C3-C4-C5	110.0442
C39-C43	1.397	H15-C14-H33	105.71	N26-C3-C4-H7	-130.791
C41-C43	1.395	C16-C14-H33	108.70	N26-C3-C4-H8	-9.911
C46-C47	1.401	C14-C16-H17	108.68	C2-C3-N26-N27	-3.8249
C46-C48	1.400	C14-C16-H18	109.47	C4-C3-N26-N27	-173.059
C47-C49	1.395	C14-C16-C19	114.89	C3-C4-C5-N9	55.7579
C48-C51	1.395	H17-C16-H18	106.01	C3-C4-C5-H34	-64.2032
C49-C53	1.396	H17-C16-C19	108.23	C3-C4-C5-C46	178.142
C51-C53	1.396	H18-C16-C19	109.18	H7-C4-C5-N9	-65.188
C58-C59	1.404	C16-C19-H20	110.08	H7-C4-C5-H34	174.8509
C58-C60	1.402	C16-C19-H21	108.50	H7-C4-C5-C46	57.1961
C59-C61	1.392	C16-C19-C22	113.13	H8-C4-C5-N9	175.5646
C60-C63	1.394	H20-C19-H21	106.93	H8-C4-C5-H34	55.6035
C61-C65	1.395	H20-C19-C22	108.84	H8-C4-C5-C46	-62.0513
C63-C65	1.396	H21-C19-C22	109.18	C4-C5-N9-C1	-58.9801

3.2. Vibrational assignments.

The 3-PDPPPHC molecule has 68 atoms and belongs to C_1 point group symmetry; hence 198 normal modes of vibrations are possible and are distributed as Γ_{vib}= 133A′+65A″. All the vibrations are active in both IR and Raman absorption. With the exclusion of the anharmonicity factor and the basis set used, certain theoretical frequencies are not matched with experimental values. Hence, in this study, a linear scaling procedure is used to scale down the harmonic frequencies; we have followed the uniform scaling factor 0.9608 for DFT method [45]. After scaling the calculated frequencies, the observed values' deviation is less than 10 cm^{-1} with few exceptions. The scaled frequencies, observed frequencies (FT-IR, FT-Raman) with their intensities, force constants, reduced masses, and proposed vibrational assignments along with TED values are summarized in Table 2. The simulated, observed FT-IR and FT-Raman spectra are shown in Figs. 2 & 3, respectively.

3.2.1. N-H vibrations.

In general, the ν_{N-H} modes are expected to occur in the region 3200-3400 cm^{-1} [46]. In agreement with these observations, the harmonic bands at 3435, 3421 & 3383 cm^{-1} (mode nos: 1, 2 & 3) is designated as ν_{N-H} mode, while the experimental FT-IR bands at 3433, 3374 & 3308 cm^{-1} and 3434, 3375 & 3310 cm^{-1} in FT-Raman spectrum and is a pure mode (TED: 92, 92 & 99%), respectively. The harmonic wavenumber for β_{NNH} & τ_{HNNC} lies at 1516/421 cm^{-1}, respectively having considerable TED value (25 & 56%) and its corresponding mode nos: 48 & 161. On comparing the present investigation with the above literature, the lowering/increasing of wavenumbers may be due to the delocalization of electrons in the piperidone ring.

3.2.2. Aromatic C-H vibrations.

Aromatic compounds commonly exhibit multiple bands in the region of 3000-3100 cm^{-1} due to CH stretching vibrations. In 3-PDPPPHC the C-H bands were observed at 3083 cm^{-1} in FT-Raman and 3084 cm^{-1} in FT-IR spectra, while the calculated frequencies are in the range of 3084 cm^{-1} (mode no: 5). In addition, C-H vibrations are observed in the region of 3057, 3030, 2949, 2930 & 2860 cm^{-1} in FT-Raman spectrum and 3058, 3028, 2948, 2925 & 2855 cm^{-1} in FT-IR spectrum and the corresponding harmonic values lies at 3057, 3042, 2950, 2934 & 2882 cm^{-1}, respectively (mode nos: 14, 18, 23, 25 & 32). These assignments are well support by their TED value.

In general, the C-H in-plane bending vibrations normally occur as a number of strong and weak bands in the region 1000-1400 cm^{-1}. Similarly, the C-H out-of-plane bending vibrations are expected in the region of 809-950 cm^{-1} [47]. In 3-PDPPPHC the C-H in-plane bending vibrations are assigned at 1444, 1382 & 1325 cm^{-1} in FT-IR spectrum and 1445, 1385 & 1328 cm^{-1} in FT-Raman spectrum and their related harmonic frequencies are: 1446, 1385 & 1328 cm^{-1} (mode nos: 51, 57, 63). The C-H out-of-plane bending vibration of 3-PDPPPHC molecule was observed at 828, 807 cm^{-1} in the FT-IR spectrum. In contrast, the Raman bands are observed at 829, 806 cm^{-1}, respectively. The calculated frequencies are 832 & 806 cm-1 (mode nos: 128, 130) also find support from TED values for the same mode.

3.2.3. C-C vibrations.

In General, the C=C and C-C stretching vibrations are usually occur in the region 1450–1625 cm^{-1} [48]. Hence in the present investigation, the FT-IR band identified at 1444 cm^{-1} and FT-Raman band at 1445 cm^{-1} is assigned to C-C stretching vibration of 3-PDPPPHC in mode no: 51 TED 25%. The β_{CCH} vibrations are assigned at 1068 cm^{-1} in FT-IR and 1030 cm^{-1} in FT-Raman spectrum. Its corresponding harmonic values lie at 1036 cm^{-1} with TED 45% (mode no: 98). Similarly, Γ_{HCCH} mode ascribed to wavenumbers at 980 cm^{-1} (mode no: 116). These assignments have considerable TED values and compare with experimental values (FT-IR/941 and FT-Raman/940 cm^{-1}), respectively. These results conclude that the positive/negative deviation of wavenumbers may be due to the piperidone ring's resonance.

3.2.4. C=N, C-N, and N-N vibrations.

In general, the identification of C=N and C-N vibrations was very difficult, as the mixing of several bands become possible in this region. Silverstain and Webster [49] assigned the C-N stretching absorption in the region 1689–1417 cm^{-1} for aromatic amines. In 3-PDPPPHC, the C=N stretching band is found at 1594 cm^{-1} in FT-IR and 1595 cm^{-1} in Raman band. The computed wavenumbers 1646 cm^{-1} (mode no: 35) are assigned with TED value of 78%. From Table 2, C-N stretching vibration is observed at 1535 cm^{-1} and 1537 cm^{-1} in FT-IR & FT-Raman bands, respectively. The DFT calculation gave bands at 1576 cm^{-1} (mode no: 41). The in-plane (β_{HNC} : FT-IR/1382 & FT-Raman/1385 cm^{-1}) and out-of-plane bending Γ_{CCNH} appeared at 1300 (FT-IR) and 1299 cm^{-1}(FT-Raman), this vibration shows in good agreement with the theoretical frequency of 1359 & 1320 cm^{-1} (mode nos: 59 & 65) by B3LYP/6-311++G(d,p) method. The theoretically computed N-N stretching has been calculated at 1115 cm^{-1}, which mode no. 93 (TED: 25%) is in agreement with FT-IR value 1109 cm^{-1} and FT-Raman 1112 cm^{-1}, respectively.

3.2.5. C=S vibrations.

In this study, the mode no: 139 are ascribed to $\nu_{C=S}$ vibrations at 698 cm^{-1} in FT-IR band and $\nu_{C=S}$/699 cm^{-1} in FT-Raman band and its corresponding harmonic wavenumbers at 672 cm^{-1} to support from TED value (>23%), respectively following the literature [50]. The harmonic frequencies 650 and 573 cm^{-1} (mode nos: 144, 152) are designated as β_{CS} (FT-IR: 645 & FT-Raman: 648 cm^{-1}) and Γ_{CS} modes (FT-IR: 570 & FT-Raman: 572 cm^{-1}), respectively. These assignments are found support from TED values >20%. It should be discussed here that the present assignment $\nu_{C=S}$ vibrations have deviated from the literature, which may be due to unhybridized orbital of sulfur-containing two electrons form part of the delocalized electron cloud by lateral overlapping with an unhybridized orbital of carbon atoms. Electron pair in one of the hybrid orbital remains shared.

3.2.6. CH_3 and CH_2 group vibrations.

Generally, the C-H stretching in alkanes occurs at lower frequencies than those of the aromatic ring (3150–3050 cm^{-1}). The CH_3 stretching is expected at 2980–2870 cm^{-1} [51], and usually, the bands are weak. In the present study, the 3-PDPPPHC possesses methyl (CH_3) and methylene (CH_2) groups. Methyl group symmetric stretching appeared at 3028 cm^{-1} in FT-IR band and at 3030 cm^{-1} in FT-Raman spectrum agree with the theoretical values of 3042 cm^{-1} (mode no: 18 by B3LYP/6-311++G(d,p) method and it has considerable TED (63%) value.

The experimental vibration bands at 1444 cm^{-1} (FT-IR) and 1445 cm^{-1} (FT-Raman) are assigned to CH_2 vibrations. The DFT value lies in the range 1446 cm^{-1} (mode no: 51) by the B3LYP method, respectively. The out-of-plane bending mode, such as wagging and twisting modes of CH_2 group, were observed at 1300, 1269 cm^{-1} (FT-IR) and 1299, 1268 cm^{-1} (FT-Raman). The DFT calculation gave the bands at 1374 and 1322 cm^{-1} (mode nos: 65 & 74). The twisting and torsion modes of methyl vibrations are identified below 500 cm^{-1} and are supported by the harmonic value with TED distribution.

3.3. Non-linear optical property.

The NLO activity provides the key functions for frequency shifting, optical modulation, optical switching, and optical logic for the developing technologies in areas such as communication, signal processing, and optical inter-connections [52]. NLO describes the behavior of media. The dielectric polarizability *'P'* responds nonlinearly to the electric field *E* of the light. In this study, the polarizability and hyperpolarizability values are calculated by DFT/6-311++G(d,p) basis set. The polarizability (α_0=0.32671x10^{-30}esu) and first-order hyperpolarizability (β_0=9.52518x10^{-30}esu) are calculated and listed in Table 3. The first order hyperpolarizability β_0 value is twenty-six times greater than that of urea. Hence, the title molecule possesses good NLO activity.

3.4. Natural bond orbital analysis.

NBO analysis is an essential tool for studying intra- and inter-molecular bonding interactions and a convenient basis for investigating charge transfer or conjugative interaction in molecular systems. Some orbitals are electron donors. Some are acceptors; the energy difference between bonding and anti-bonding orbitals makes the molecule susceptible to interactions [53]. The interactions result in a loss of occupancy from the localized NBO of the

idealized Lewis structure into an empty non-Lewis orbital. For each donor (i) and acceptor (j), the stabilization energy $E^{(2)}$ associated with the delocalization i, j is estimated as

$$E^{(2)} = \Delta E_{ij} = q_i \frac{F(i,j)^2}{\varepsilon_j - \varepsilon_i}$$

Where q_i is the donor orbital occupancy, ε_i and ε_j are diagonal elements. F(i,j) is the off-diagonal NBO Fock matrix element. The larger the energy difference $E^{(2)}$ value, the more intensive the interaction is, i.e., more is donating tendency of an electron from one orbital. More is the accepting tendency of another orbital, which makes the interaction between them stronger. The analysis of the various donors and acceptors indicate that there are only two types of donors σ & π, and two types of acceptors σ* & π*, respectively. Comparable with σ-σ*, π-π* transfer more energies in the present system.

The $E^{(2)}$ energy values and types of the transition are shown in Table 4. The hyperconjugative interactions π(C37-C39)→π*(C36-C38), π(C41-C43)→π*(C51-C53) and π(C47-C49)→π*(C46-C48) transfer more stabilization energy: 86.94, 87.11 and 87.03 KJ/mol to the molecular system. In 3-PDPPPHC, the lone pair of sulfur and nitrogen atoms play a great role, i.e., the S31, N28, and N27 atoms transfer maximum energy 55.48, 224.26, and 238.28 KJ/mol to (N27-C32, (CS31-C32) & (S31-C32) bonds, respectively. Also, the π*-π* bond also transfers more energies to its anti-bonding orbitals. The maximum hyperconjugative $E^{(2)}$ energy is exhibited during the intermolecular interaction, which leads the molecule towards medicinal and biological applications [53].

3.5. HOMO-LUMO analysis.

The HOMO and the LUMO are named as frontier molecular orbitals (FMOs). The FMOs play an important role in the optical and electric properties and quantum chemistry. The HOMO-LUMO orbitals of 3-PDPPPHC molecule are calculated in the gas phase using the DFT method with B3LYP/6-311++G(d,p) Fig. 4. The green and red colors represent the positive phase and negative phase, respectively. It is clear from the figure that the HOMO is located over thiosemicarbazone moiety, and LUMO is located over the entire molecule except for CH_2 and CH_3 groups. The calculated energy values of HOMO, LUMO and HUMO-1, LUMO+1 are -5.249 eV, -0.951 eV and -5.527 eV, -0.368 eV, respectively. The energy gap value between the HOMO and LUMO is 4.298 eV, and HOMO-1 and LUMO+1 is 5.159 eV, respectively. The energy values of HOMO (π-donor) and LUMO (π-acceptor) and their energy gap reflect the molecule's chemical activity. The physicochemical properties such as Ionization potential (IP), Electron affinity (EA), electronegativity (χ), hardness (η) and Electrophilicity index (ω) are deduced from ionization potential and electron affinity values [53] using the following equations:

Electronegativity (χ) = $-\frac{IP+EA}{2}$

Chemical hardness (μ) = $-\frac{IP-EA}{2}$ and

Electrophilicity index (ω) = $\frac{x2}{2\eta}$

The energy values of highest occupied molecular orbital (HOMO)-Lowest unoccupied molecular orbital (LUMO), energy gap, electron affinity, electrophilicity index, chemical potential, and hardness of the title molecule are listed in Table 5.

3.6. Density of states.

The density of states (DOS) spectrum for 3-PDPPPHC was obtained using Gauss Sum 3.0 program [40] and is shown in Fig. 5. The spectrum is used to explain the contribution of electrons to the conduction and valence band. The spectrum gives an idea about how many states are available at certain energy states. The lines at the starting end of the plot's energy axis, from -20 eV to -5 eV, are called filled orbital, and from -5 eV to 0 eV, they are called a virtual orbital. The virtual orbital is not occupied and is also called an acceptor orbital. In contrast, the filled orbital is called the donor orbital.

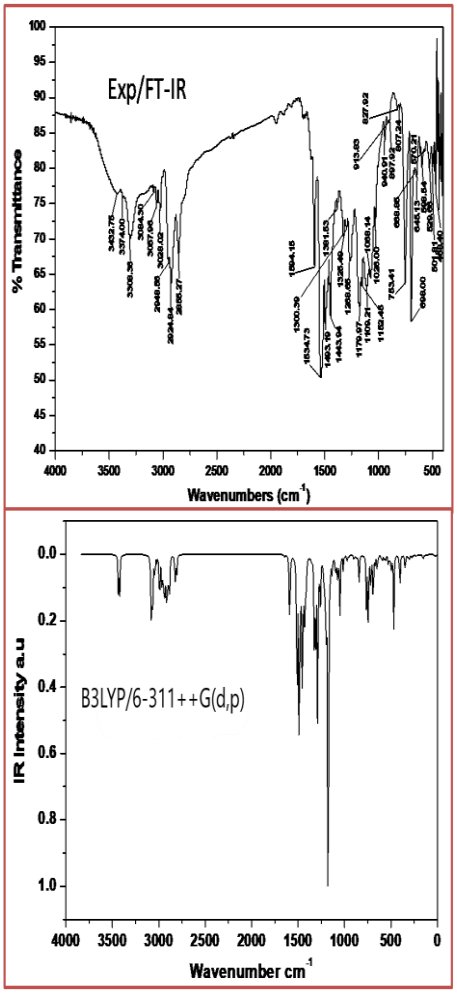

Figure 2. The theoretical and experimental FT-IR spectra of 3-PDPPPHC.

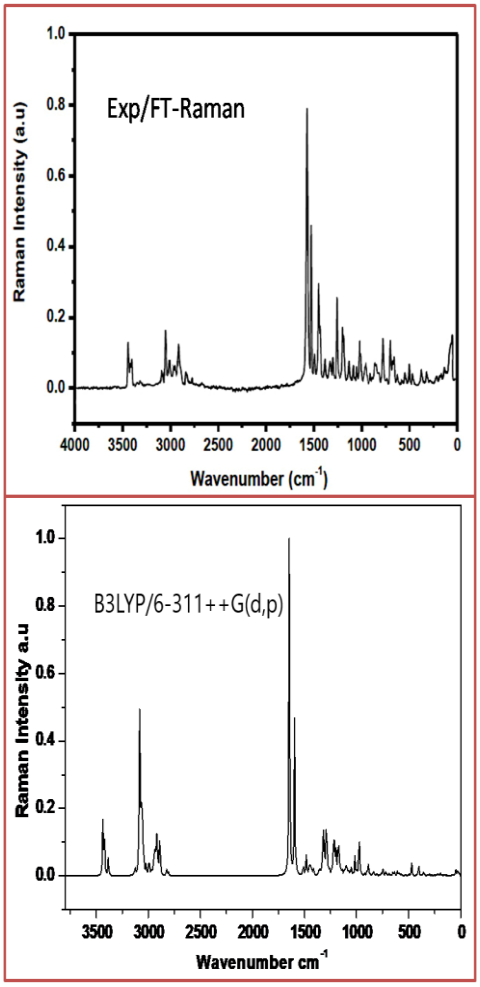

Figure 3. The theoretical and experimental FT-Raman spectra of 3-PDPPPHC.

A high-intensity DOS at specific energy levels means that there are many states available for occupation. A DOS of zero intensity means that the system can occupy no states. The variation in the peak height is due to electrons' movement between the C=C and C-C in the ring of the molecule. The peak at certain energies decreases from the value due to electrons' movement between the C=C and C-C in the ring of the molecule.

3.7. Molecular electrostatic potential analysis.

In this study, a 3D MEP, ESP, and TD plot of 3-PDPPPHC molecule are shown in Fig. 6. In MEP map, the maximum positive/negative regions are preferred sites for nucleophilic/electrophilic attack. They are represented by Blue/Red color, respectively. The

importance of MEP lies in the fact that it simultaneously displays molecular size, shape, and positive, negative, and neutral electrostatic potential regions in terms of color grading (Fig. 6) and is very useful in research of molecular structure with its physiochemical property relationship [54]. The Potential increases in the order: red < orange < yellow < green < blue. In this study, the electrostatic potential plot is based on the ED distribution within the molecule at different points. The lone pair atoms (sulfur & nitrogen) and hydrogen atoms in thiosemicarbazone are covered respectively by Red and blue regions. At the same time, the rest of the molecule is neutral. The positive and negative potential of the 3-PDPPPHC molecule ranges from -6.681e^{-2} a.u to 6.681e^{-2} a.u. These two ends of the molecule, which are positively and negatively charged, are prone to the electrophilic and nucleophilic attack of the title molecule.

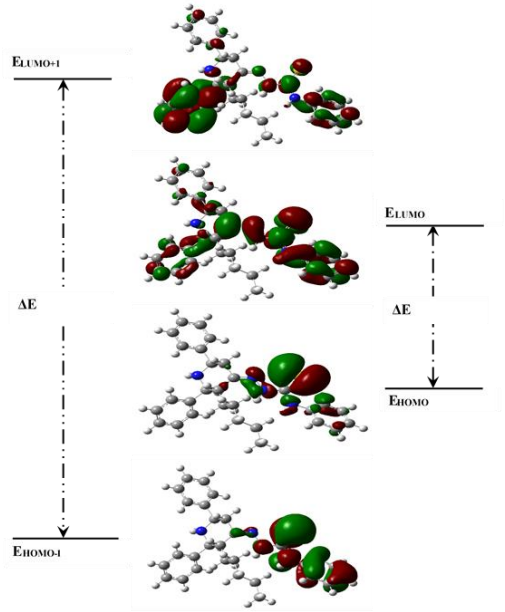

Figure 4. Frontier molecular orbitals of 3-PDPPPHC.

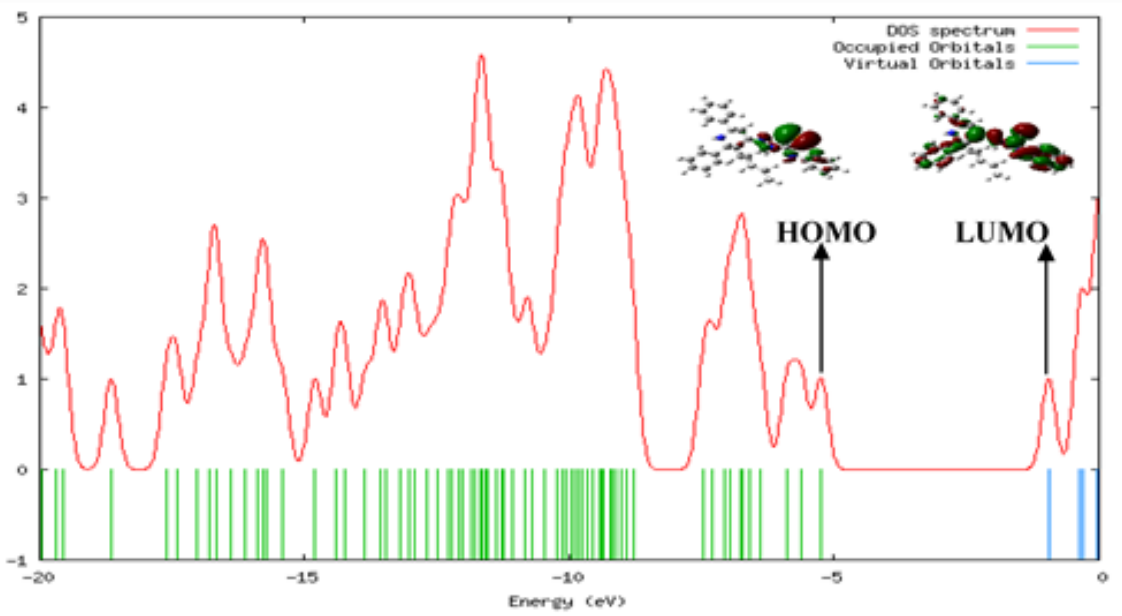

Figure 5. Density of states (DOS) diagrams for 3-PDPPPHC.

Table 2. The vibrational assignments of 3-PDPPPHC.

Mode No	Observed Frequencies (cm^{-1})		Calculated Frequencies (cm^{-1})		IR Intensity		Raman Intensity		Vibrational Assignments
	FT-IR	FT-Raman	Un Scaled	Scaled[a]	Abs.	Rel[b].	Abs.	Rel[c].	TED≥10%[d]
1	3433	3434	3575	3435	49.82	19.71	358.58	100.00	$VN_{28}H_{29}(92)$
2	3374	3375	3561	3421	54.09	21.40	219.94	61.34	$VN_{27}H_{30}(92)$
3	3308	3310	3521	3383	0.42	0.17	107.60	30.01	$VN_{9}H_{10}(99)$
4			3256	3128	0.99	0.39	43.74	12.20	$VC_{60}H_{64}(98)$
5	3084	3083	3210	3084	13.15	5.20	327.00	91.19	$VC_{47}H_{64}(63)+VC_{60}H_{64}(16)$
6			3210	3084	6.69	2.65	156.45	43.63	$VC_{37}H_{40}(47)+VC_{39}H_{44}(21)+VC_{43}H_{57}(16)$
7			3209	3083	29.74	11.77	329.42	91.87	$VC_{61}H_{66}(24)+VC_{63}H_{67}(16)+VC_{65}H_{68}(58)$
8			3203	3077	13.65	5.40	166.32	46.38	$VC_{37}H_{40}(25)+VC_{41}H_{45}(22)+VC_{43}H_{57}(25)+VC_{53}H_{56}(10)$
9			3203	3077	45.85	18.14	99.49	27.74	$VC_{47}H_{50}(25)+VC_{51}H_{55}(22)+VC_{53}H_{56}(10)$
10			3194	3069	24.85	9.83	105.08	29.30	$VC_{61}H_{66}(51)+ VC_{63}H_{67}(40)$
11			3192	3067	22.11	8.75	96.55	26.93	$VC_{38}H_{42}(10)+VC_{39}H_{44}(27)+VC_{41}H_{45}(40)+VC_{43}H_{57}(14)$
12			3191	3066	21.72	8.59	105.04	29.29	$VC_{48}H_{52}(13)+VC_{49}H_{54}(26)+VC_{51}H_{55}(36)+VC_{53}H_{56}(19)$
13			3185	3060	0.02	0.01	91.52	25.52	$VC_{61}H_{66}(14)+VC_{63}H_{67}(42)+VC_{65}H_{68}(38)$
14	3058	3057	3182	3057	0.16	0.06	91.16	25.42	$VC_{38}H_{42}(12)+VC_{39}H_{44}(47)+VC_{43}H_{57}(31)$
15			3180	3055	0.62	0.25	103.08	28.75	$VC_{48}H_{52}(20)+VC_{49}H_{54}(49)+VC_{53}H_{56}(25)$
16			3173	3049	5.87	2.32	20.79	5.80	$VC_{48}H_{52}(62)+VC_{51}H_{55}(23)$
17			3172	3048	6.84	2.71	23.95	6.68	$VC_{38}H_{42}(73)+VC_{41}H_{45}(19)$
18	3028	3030	3166	3042	16.18	6.40	65.88	18.37	$VC_{22}H_{24}(63)+VC_{22}H_{25}(33)$
19			3144	3021	6.25	2.47	44.47	12.40	$VC_{4}H_{8}(88)+VC_{4}H_{7}(12)$
20			3115	2993	35.20	13.93	60.81	16.96	$VC_{59}H_{62}(88)+VC_{61}H_{66}(10)$
21			3113	2991	40.19	15.90	51.90	14.47	$VC_{22}H_{23}(59)+VC_{22}H_{25}(28)$
22			3087	2966	55.71	22.05	31.51	8.79	$VC_{11}H_{12}(63)+VC_{14}H_{15}(19)+VC_{14}H_{33}(11)$
23	2948	2949	3070	2950	31.11	12.31	40.89	11.40	$VC_{11}H_{12}(14)+VC_{14}H_{15}(13)+VC_{16}H_{17}(36)+VC_{16}H_{18}(24)$
24			3065	2945	23.56	9.32	72.15	20.12	$VC_{11}H_{12}(18)+VC_{14}H_{15}(22)+VC_{14}H_{33}(35)+VC_{16}H_{17}(19)$
25	2925	2930	3054	2934	36.20	14.33	95.62	26.67	$VC_{4}H_{8}(12)+VC_{4}H_{7}(86)$
26			3042	2923	33.58	13.29	132.97	37.08	$VC_{22}H_{23}(34)+VC_{22}H_{24}(29)+VC_{22}H_{25}(35)$
27			3036	2917	4.59	1.82	98.45	27.46	$VC_{19}H_{20}(51)+VC_{19}H_{21}(20)$
28			3035	2916	31.01	12.27	46.07	12.85	$VC_{2}H_{6}(10)+VC_{14}H_{15}(34)+VC_{14}H_{33}(32)$
29			3026	2907	11.10	4.39	28.99	8.08	$VC_{2}H_{6}(61)+VC_{16}H_{18}(11)$
30			3024	2905	48.80	19.31	26.78	7.47	$VC_{16}H_{17}(29)+VC_{16}H_{18}(53)$
31			3010	2892	22.39	8.86	142.31	39.69	$VC_{2}H_{6}(17)+VC_{11}H_{13}(66)+VC_{19}H_{21}(14)$
32	2855	2860	3000	2882	37.04	14.66	71.82	20.03	$VC_{11}H_{13}(10)+VC_{19}H_{20}(30)+VC_{19}H_{21}(55)$
33			2940	2825	36.57	14.47	38.49	10.74	$VC_{5}H_{34}(98)$
34			2923	2808	33.45	13.24	26.61	7.42	$VC_{1}H_{35}(98)$
35	1594	1595	1713	1646	2.57	1.02	1282.17	357.57	$VN_{26}C_{3}(78)$
36			1662	1597	4.86	1.92	108.43	30.24	$VC_{48}C_{51}(31)+VC_{53}C_{49}(14)+\beta C_{51}C_{53}C_{49}(14)$
37			1660	1595	5.35	2.12	91.31	25.47	$\beta C_{36}C_{37}C_{39}(13)+VC_{38}C_{41}(37)+VC_{43}C_{39}(10)$
38			1660	1595	50.28	19.90	343.94	95.92	$VC_{60}C_{63}(19)+VC_{59}C_{61}(16)+VC_{65}C_{61}(12)+\beta C_{59}C_{58}C_{60}(12)$

39			1651	1586	29.82	11.80	3.88	1.08	$VC_{63}C_{65}(22)+VC_{65}C_{61}(18)+\beta C_{58}C_{60}C_{60}(19)+\beta C_{60}C_{63}C_{65}(11)$
40			1641	1577	1.91	0.76	12.47	3.48	$VC_{51}C_{53}(25)+VC_{46}C_{48}(16)$
41	1535	1537	1640	1576	0.36	0.14	5.36	1.49	$VN_{29}C_{50}(38)+VC_{43}C_{39}(19)+VC_{36}C_{37}(18)$
42	1493	1492	1574	1512	247.38	97.89	48.78	13.60	$\beta H_{29}N_{28}C_{32}(54)$
43			1553	1492	179.92	71.20	9.55	2.66	$\beta H_{30}N_{27}N_{26}(40)+\beta H_{12}C_{11}H_{13}(54)$
44			1541	1481	99.23	39.27	76.29	21.28	$\beta H_{64}C_{60}C_{63}(12)+\beta H_{62}C_{59}C_{61}(20)+\beta H_{66}C_{61}C_{59}(14)+\beta H_{67}C_{63}C_{60}(19)$
45			1538	1478	17.09	6.76	3.54	0.99	$\beta H_{50}C_{47}C_{46}(13)+\beta H_{52}C_{48}C_{51}(16)+\beta H_{54}C_{49}C_{53}(18)+\beta H_{55}C_{51}C_{53}(17)$
46			1536	1476	14.02	5.55	0.91	0.25	$\beta H_{40}C_{37}C_{39}(15)+\beta H_{42}C_{38}C_{41}(16)+\beta H_{44}C_{39}C_{43}(18)+\beta H_{45}C_{41}C_{38}(17)$
47			1526	1466	15.38	6.09	0.82	0.23	$\beta H_{23}C_{22}H_{25}(19)+\beta H_{20}C_{19}H_{21}(50)$
48			1516	1457	123.33	48.80	6.93	1.93	$\beta H_{30}N_{27}N_{26}(25)+\beta H_{12}C_{11}H_{13}(28)+\beta H_{15}C_{14}H_{33}(25)$
49			1513	1454	6.76	2.67	15.30	4.27	$\beta H_{23}C_{22}C_{19}(25)+\Gamma C_{22}H_{23}C_{19}H_{24}(65)$
50			1511	1452	0.93	0.37	25.91	7.22	$\beta H_{23}C_{22}C_{22}(35)+\beta H_{15}C_{14}H_{33}(13)+\Gamma C_{22}H_{23}C_{19}H_{25}(10)$
51	1444	1445	1505	1446	68.31	27.03	5.32	1.48	$VC_{51}C_{53}(25)+\beta H_{12}C_{11}H_{13}(13)+\beta H_{15}C_{14}H_{33}(47)$
52			1501	1442	1.83	0.72	24.76	6.90	$\beta H_{17}C_{16}H_{18}(73)+\beta H_{20}C_{19}H_{21}(20)$
53			1497	1438	9.37	3.71	1.97	0.55	$\beta H_{54}C_{49}C_{53}(11)+\beta H_{55}C_{51}C_{53}(12)+\beta H_{56}C_{53}C_{51}(26)$
54			1496	1437	8.38	3.32	2.05	0.57	$\beta H_{36}C_{37}C_{39}(11)+\beta H_{44}C_{39}C_{43}(10)+\beta H_{45}C_{41}C_{38}(10)+\beta H_{57}C_{43}C_{41}(25)$
55			1488	1430	41.12	16.27	9.74	2.71	$\beta H_{29}N_{28}C_{32}(10)+\beta H_{7}C_{4}H_{8}(26)+\beta H_{66}C_{61}C_{59}(11)+\beta H_{68}C_{65}C_{63}(16)$
56			1484	1426	63.00	24.93	13.25	3.70	$\beta H_{7}C_{4}H_{8}(55)$
57			1469	1411	42.75	16.92	26.17	7.30	$\beta H_{10}N_{9}C_{5}(73)$
58			1429	1373	1.50	0.59	4.14	1.16	$\beta H_{24}C_{22}C_{19}(36)+\beta H_{23}C_{22}H_{25}(29)+\Gamma C_{22}H_{23}C_{19}H_{25}(31)$
59	1382	1385	1414	1359	2.73	1.08	17.39	4.85	$\beta H_{6}C_{2}H_{11}(23)+\beta H_{34}C_{5}N_{9}(21)$
60			1409	1354	2.63	1.04	8.70	2.43	$\beta H_{34}C_{5}N_{9}(13)+\beta H_{15}C_{14}C_{11}(20)$
61			1404	1349	1.06	0.42	2.21	0.62	$\beta H_{20}C_{19}C_{22}(13)+\beta C_{16}H_{17}C_{14}H_{18}(36)$
62			1401	1346	1.62	0.64	6.67	1.86	$\beta H_{20}C_{19}C_{22}(21)+\beta H_{20}C_{19}C_{22}(12)+\Gamma C_{16}H_{17}C_{14}H_{18}(14)$
63	1325	1328	1384	1330	11.24	4.45	42.85	11.95	$\beta H_{35}C_{1}C_{36}(42)$
64			1378	1324	124.68	49.34	15.66	4.37	$VN_{28}C_{32}(14)+\beta H_{64}C_{60}C_{63}(10)+\beta H_{62}C_{59}C_{61}(12)$
65	1300	1299	1374	1320	12.83	5.08	140.20	39.10	$\Gamma C_{1}C_{2}C_{36}H_{35}(23)+\Gamma C_{5}C_{46}N_{9}H_{34}(33)$
66			1363	1310	80.22	31.74	44.71	12.47	$VC_{60}C_{63}(24)+VC_{59}C_{61}(32)$
67			1361	1308	1.97	0.78	3.16	0.88	$VC_{53}C_{49}(27)+VC_{46}C_{48}(15)+\beta H_{50}C_{47}C_{46}(18)+\beta H_{52}C_{48}C_{51}(19)$
68			1360	1307	0.20	0.08	1.66	0.46	$VC_{41}C_{43}(26)+VC_{36}C_{37}(17)+\beta H_{40}C_{37}C_{39}(17)+\beta H_{42}C_{38}C_{41}(19)$
69			1352	1299	1.59	0.63	8.19	2.28	$\beta H_{12}C_{11}C_{14}(18)+\beta H_{17}C_{16}C_{14}(20)+\beta H_{20}C_{19}C_{22}(11)$
70			1346	1293	95.14	37.65	119.17	33.23	$VN_{28}C_{32}(15)+VN_{28}C_{58}(12)+\beta H_{64}C_{60}C_{63}(14)$
71			1345	1292	82.09	32.48	14.42	4.02	$\beta H_{12}C_{11}C_{14}(11)+\tau H_{33}C_{14}C_{16}C_{19}(15)$
72			1336	1284	18.61	7.36	68.44	19.09	$VC_{46}C_{48}(10)$
73			1333	1281	21.83	8.64	21.83	6.09	$\beta H_{17}C_{16}C_{14}(13)+\Gamma C_{1}C_{2}C_{36}H_{35}(13)+\tau H_{18}C_{16}C_{19}H_{21}(10)$
74	1269	1268	1322	1270	18.52	7.33	18.80	5.24	$\beta H_{12}C_{11}C_{14}(10)+\tau H_{18}C_{16}C_{19}H_{21}(17)$
75			1311	1260	48.91	19.35	10.10	2.82	$\beta H_{17}C_{16}C_{14}(15)$
76			1310	1259	14.42	5.71	6.57	1.83	$\beta H_{15}C_{14}C_{11}(10)+\beta H_{20}C_{19}C_{22}(17)$
77			1291	1240	2.22	0.88	8.72	2.43	$\beta H_{34}C_{5}N_{9}(10)+\tau H_{8}C_{4}C_{3}N_{26}(22)+\tau H_{7}C_{4}C_{3}H_{2}(12)$
78			1279	1229	5.90	2.34	11.08	3.09	$\tau H_{18}C_{16}C_{19}H_{21}(11)$
79			1268	1218	48.49	19.19	207.65	57.91	$VC_{60}C_{63}(11)+\beta C_{58}C_{60}C_{63}(12)+VN_{28}C_{58}(13)$
80			1253	1204	49.30	19.51	35.93	10.02	$\tau H_{6}C_{2}C_{3}C_{4}(27)$
81			1245	1196	66.86	26.46	70.73	19.72	$\beta H_{7}C_{4}C_{3}(11)$

82	1180	1180	1229	1181	221.27	87.56	18.18	5.07	$VN_{27}C_{32}(16)$
83			1223	1175	252.70	100.00	86.21	24.04	$VC_{46}C_{5}(18)$
84			1221	1173	126.58	50.09	54.18	15.11	$VC_{36}C_{1}(21)$
85			1209	1162	2.63	1.04	14.14	3.94	$\beta H_{64}C_{60}C_{63}(20)+\beta H_{62}C_{59}C_{61}(21)+\beta H_{66}C_{61}C_{59}(15)+\beta H_{67}C_{63}C_{60}(18)$
86			1207	1160	5.61	2.22	10.96	3.06	$\tau C_{14}C_{11}C_{16}H_{15}(13)$
87			1204	1157	7.78	3.08	5.69	1.59	$\beta H_{42}C_{38}C_{41}(11)+\beta H_{52}C_{48}C_{51}(11)$
88	1152	1153	1202	1155	3.27	1.29	4.76	1.33	$\beta H_{42}C_{38}C_{41}(12)+\beta H_{52}C_{48}C_{51}(12)+\beta H_{55}C_{51}C_{53}(10)$
89			1187	1140	0.83	0.33	8.95	2.50	$\beta H_{66}C_{61}C_{59}(22)+\beta H_{67}C_{63}C_{60}(18)+\beta H_{68}C_{65}C_{63}(35)$
90			1187	1140	0.04	0.02	6.93	1.93	$\beta H_{44}C_{39}C_{43}(19)+\beta H_{45}C_{41}C_{38}(15)+\beta H_{57}C_{43}C_{41}(33)$
91			1187	1140	1.89	0.75	5.61	1.57	$VC_{53}C_{49}(10)+\beta H_{54}C_{49}C_{53}(19)+\beta H_{55}C_{51}C_{53}(14)+\beta H_{56}C_{53}C_{51}(32)$
92			1181	1135	20.27	8.02	6.19	1.73	$\beta H_{7}C_{4}C_{3}(13)$
93	1109	1112	1160	1115	1.62	0.64	27.05	7.54	$VN_{27}N_{26}(25)$
94			1145	1100	14.56	5.76	31.48	8.78	$VN_{27}N_{26}(13)$
95			1134	1090	22.19	8.78	27.38	7.64	$VN_{9}C_{5}(41)+ VC_{4}C_{5}(10)$
96			1119	1075	19.58	7.75	9.09	2.53	$VN_{27}N_{26}(11)+\Gamma C_{11}C_{2}C_{14}H_{12}(10)$
97			1115	1071	8.97	3.55	1.73	0.48	$\beta H_{68}C_{65}C_{63}(11)$
98	1068	1067	1114	1070	0.52	0.21	1.77	0.49	$\beta H_{55}C_{51}C_{53}(45)$
99			1105	1062	3.82	1.51	6.89	1.92	$\beta H_{56}C_{53}C_{51}(30)$
100			1095	1052	3.89	1.54	7.26	2.02	$VC_{11}C_{2}(14)$
101			1094	1051	62.39	24.69	16.96	4.73	$VC_{4}C_{3}(13)+VN_{9}C_{1}(20)+VC_{11}C_{2}(11)$
102	1025	1030	1078	1036	0.80	0.32	7.14	1.99	$VC_{14}C_{11}(10)+VC_{16}C_{14}(33)+ VC_{19}C_{16}(25)$
103			1057	1016	8.30	3.29	16.61	4.63	$VC_{63}C_{65}(25)+VC_{65}C_{61}(23)$
104			1056	1015	2.86	1.13	35.69	9.95	$VC_{41}C_{43}(10)+VC_{51}C_{53}(10)$
105			1055	1014	8.53	3.37	8.07	2.25	$VC_{41}C_{43}(17)+VC_{43}C_{39}(12)$
106			1039	998	1.21	0.48	8.32	2.32	$VC_{22}C_{19}(43)+VC_{14}C_{11}(13)$
107			1018	978	1.09	0.43	5.18	1.44	$VC_{22}C_{19}(11)$
108			1017	977	1.81	0.72	60.53	16.88	$\beta C_{38}C_{41}C_{43}(11)$
109			1016	976	1.04	0.41	14.78	4.12	$\beta C_{41}C_{43}C_{39}(11)+\beta C_{38}C_{41}C_{43}(16)$
110			1014	974	0.20	0.08	73.54	20.51	$\beta C_{60}C_{63}C_{65}(17)+\beta C_{63}C_{65}C_{61}(20)+\beta C_{65}C_{61}C_{59}(35)$
111			1010	970	5.18	2.05	8.94	2.49	$\beta C_{63}C_{65}C_{61}(22)$
112			1003	964	0.32	0.13	1.50	0.42	$\tau H_{40}C_{37}C_{39}H_{44}(22)+\tau H_{42}C_{38}C_{41}H_{45}(12)+\Gamma C_{43}C_{39}C_{41}H_{57}(14)$
113			1002	963	0.26	0.10	0.46	0.13	$\tau H_{40}C_{37}C_{39}H_{44}(16)+\Gamma C_{43}C_{39}C_{41}H_{57}(12)+\tau H_{50}C_{47}C_{49}H_{54}(23)$
114			997	958	2.69	1.07	4.61	1.28	$\Gamma C_{53}C_{49}C_{51}H_{56}(10)$
115			990	951	0.59	0.23	1.92	0.54	$\Gamma C_{60}C_{58}C_{63}H_{64}(10)+\tau H_{62}C_{59}C_{61}H_{66}(13)+H_{64}C_{60}C_{63}H_{67}(51)$
116	941	940	980	942	0.18	0.07	0.38	0.11	$\Gamma H_{42}C_{38}C_{41}H_{45}(11)+\tau H_{50}C_{47}C_{49}H_{54}(26)+\tau H_{52}C_{48}C_{51}H_{55}(40)$
117			978	940	0.55	0.22	0.22	0.06	$\tau H_{40}C_{37}C_{39}H_{44}(30)+\tau H_{42}C_{38}C_{41}H_{45}(40)+\tau H_{52}C_{48}C_{51}H_{55}(10)$
118			961	923	0.31	0.12	1.12	0.31	$\tau H_{62}C_{59}C_{61}H_{66}(56)+\tau H_{64}C_{60}C_{63}H_{67}(29)$
119	913		959	921	0.17	0.07	6.47	1.80	$VC_{14}C_{11}(16)+VC_{2}C_{1}(15)$
120			937	900	4.91	1.94	6.45	1.80	$\tau H_{50}C_{47}C_{49}C_{53}(18)+\Gamma C_{48}C_{46}C_{51}H_{52}(16)+\Gamma C_{53}C_{49}C_{51}H_{56}(23)$
121	898		936	899	3.03	1.20	10.25	2.86	$\Gamma C_{37}C_{36}C_{39}H_{40}(16)+\Gamma C_{38}C_{36}C_{41}H_{42}(16)+\Gamma C_{43}C_{39}C_{41}H_{57}(21)$
122			924	888	1.03	0.41	37.35	10.42	$VC_{4}C_{5}$ (28)
123			915	879	2.06	0.81	4.11	1.15	$VC_{2}C_{1}(18)$
124			906	870	3.45	1.37	1.88	0.52	$\Gamma C_{60}C_{58}C_{63}H_{64}(29)+\tau H_{62}C_{59}C_{61}C_{65}(14)+ \tau H_{62}C_{59}C_{61}H_{66}(10)$

125			890	855	2.00	0.79	2.62	0.73	$VC_{19}C_{16}$ (10)+$\Gamma C_{16}C_{14}C_{19}H_{17}$(14)
126			879	845	35.75	14.15	7.33	2.05	$VN_{28}C_{58}$(10)+ $\beta C_{63}C_{65}C_{61}$(16)
127			868	834	0.91	0.36	8.21	2.29	$\Gamma C_{37}C_{36}C_{39}H_{40}$(21)+$\Gamma C_{38}C_{36}C_{41}H_{42}$(22)+$\tau H_{50}C_{47}C_{49}C_{53}$(23)
128	828	829	866	832	0.18	0.07	1.98	0.55	$\Gamma C_{37}C_{36}C_{39}H_{40}$(24)+$\Gamma C_{38}C_{36}C_{41}H_{42}$(24)+$\tau H_{50}C_{47}C_{49}C_{53}$(23)
129			855	821	0.33	0.13	3.11	0.87	$\Gamma C_{16}C_{14}C_{19}H_{17}$(16)
130	807	806	839	806	0.15	0.06	4.46	1.24	$\Gamma C_{48}C_{46}C_{51}H_{52}$(23)
131			835	802	0.55	0.22	4.60	1.28	$\Gamma C_{60}C_{58}C_{63}H_{64}$(37)+$\tau H_{62}C_{59}C_{61}C_{65}$(49)
132			811	779	1.11	0.44	2.95	0.82	VC_2C_3 (15)
133	753	755	796	765	56.23	22.25	4.72	1.32	$\Gamma N_9C_1C_5H_{10}$(46)
134			780	749	12.36	4.89	13.29	3.71	$\Gamma C_{53}C_{49}C_{51}H_{56}$(10)
135			779	748	4.01	1.59	2.16	0.60	$\Gamma C_{16}C_{14}C_{19}H_{17}$(15)
136			776	746	65.62	25.97	5.83	1.63	$\Gamma C_{43}C_{39}C_{41}H_{57}$(12)
137			773	743	21.88	8.66	4.29	1.20	$VS_{31}C_{32}$ (10)+$\tau H_{68}C_{65}C_{61}C_{59}$(19)+$\tau N_{28}C_{58}C_{60}C_{59}$(17)
138			751	722	11.66	4.61	1.18	0.33	$\Gamma C_{16}C_{14}C_{19}H_{17}$(27)+$\Gamma C_{19}C_{16}C_{22}H_{20}$(32)
139	698	699	747	718	36.27	14.35	18.70	5.22	$VS_{31}C_{32}$(23)
140			722	694	38.07	15.07	2.14	0.60	$\tau C_{39}C_{37}C_{43}C_{41}$(22)
141			718	690	17.69	7.00	1.81	0.50	$\tau C_{38}C_{41}C_{39}C_{43}$(15)+$\tau C_{36}C_{38}C_{43}C_{41}$(47)+$\tau C_{39}C_{37}C_{43}C_{41}$(20)
142			715	687	10.43	4.13	3.85	1.07	$\tau C_{46}C_{48}C_{53}C_{51}$(41)+$\tau C_{48}C_{51}C_{49}C_{53}$(10)+$\tau C_{49}C_{47}C_{53}C_{51}$(11)
143	669	670	699	672	10.10	4.00	0.87	0.24	$\tau H_{62}C_{59}C_{61}C_{65}$(10)+$\tau H_{68}C_{65}C_{61}C_{59}$(10)+$\tau C_{58}C_{60}C_{65}C_{63}$(45)
144	645	648	676	650	22.84	9.04	14.00	3.90	$\beta N_{27}C_{32}S_{31}$ (24)
145			661	635	1.34	0.53	8.96	2.50	$\beta C_{48}C_{51}C_{53}$(40)
146			635	610	0.38	0.15	5.67	1.58	$\beta C_{46}C_{47}C_{49}$(18)+$\beta C_{48}C_{51}C_{53}$(44)+$\beta C_{53}C_{49}C_{47}$(13)
147			634	609	0.02	0.01	3.69	1.03	$\beta C_{36}C_{38}C_{41}$(20)+$\beta C_{43}C_{39}C_{37}$(37)
148	599	600	631	606	2.63	1.04	5.41	1.51	$\beta C_{58}C_{60}C_{63}$(22)+$\beta C_{60}C_{63}C_{65}$(33)+$\beta C_{65}C_{61}C_{59}$(25)
149			620	596	7.12	2.82	6.14	1.71	$\beta C_{47}C_{46}C_{48}$(14)
150			614	590	2.16	0.86	4.58	1.28	$\Gamma S_{31}N_{27}N_{28}C_{32}$(16)
151			601	577	2.74	1.09	1.97	0.55	$\Gamma S_{31}N_{27}N_{28}C_{32}$(36)
152	570	572	596	573	3.28	1.30	3.95	1.10	$\Gamma S_{31}N_{27}N_{28}C_{32}$(22)
153			583	560	9.60	3.80	1.59	0.44	$\beta C_2C_1N_9$(16)
154	529	528	551	529	10.98	4.34	2.72	0.76	$\beta C_4C_5N_9$(14)
155			540	519	8.50	3.36	1.25	0.35	$\beta C_4C_5N_9$(10)
156	501	500	520	500	18.61	7.37	3.14	0.87	$\tau H_{29}N_{28}C_{58}C_{60}$(21)+$\tau C_{61}C_{59}C_{65}C_{63}$(11)+$\Gamma S_{31}N_{27}N_{28}C_{32}$(37)
157			512	492	8.15	3.22	4.03	1.12	$\Gamma N_{28}C_{58}C_{60}C_{59}$(18)
158	468	470	490	471	79.83	31.59	32.99	9.20	$\tau H_{29}N_{28}C_{58}C_{60}$(56)
159			481	462	2.24	0.89	0.97	0.27	$\beta C_{22}C_{19}C_{16}$(11)+$\beta C_{19}C_{16}C_{14}$(10)
160			438	421	1.47	0.58	1.89	0.53	$\beta C_4C_3C_2$(29)
161			421	404	42.59	16.85	32.14	8.96	$\tau H_{30}N_{27}N_{26}C_3$(51)
162			419	403	2.75	1.09	1.57	0.44	$\tau C_{30}C_{27}C_{26}C_3$(30)+$\tau C_{39}C_{37}C_{43}C_{41}$(42)
163			418	402	0.43	0.17	0.27	0.07	$\tau C_{48}C_{51}C_{49}C_{53}$(37)+$\tau C_{49}C_{47}C_{53}C_{51}$(42)
164			417	401	0.32	0.13	1.95	0.54	$\tau C_{60}C_{63}C_{61}C_{65}$(35)+$\tau C_{60}C_{63}C_{61}C_{65}$(42)
165		378	393	378	1.37	0.54	3.26	0.91	$\beta C_3C_2C_{11}$(22)
166			371	356	1.37	0.54	11.20	3.12	$\tau C_3C_2C_4C_5$(10)+$\Gamma C_{11}C_1C_3C_2$(18)
167			361	347	22.77	9.01	3.92	1.09	$\tau H_{30}N_{27}N_{26}C_3$(15)+ $\tau C_2C_3N_{26}N_{27}$(23)

168		324	339	326	1.18	0.47	1.29	0.36	$\beta C_{60}C_{58}N_{28}(23)+\beta N_{28}C_{32}N_{27}(10)$
169			323	310	7.49	2.96	3.33	0.93	$\beta C_3C_2C_{11}(14)$
170			310	298	3.32	1.32	3.53	0.98	$\beta C_{48}C_{46}C_5(11)+\tau C_1N_9C_4C_5(14)$
171			293	282	2.20	0.87	2.20	0.61	$\beta C_{38}C_{36}C_1(14)+\beta C_{48}C_{46}C_5(12)$
172			281	270	3.75	1.49	1.38	0.38	$\beta C_{22}C_{19}C_{16}(11)$
173			263	253	1.29	0.51	2.29	0.64	$\beta C_{22}C_{19}C_{16}(23)+\beta C_{19}C_{16}C_{14}(21)$
174			249	239	0.27	0.11	0.30	0.08	$\tau H_{23}C_{22}C_{19}C_{16}(52)$
175		232	243	233	1.17	0.46	4.44	1.24	$\tau C_{60}C_{63}C_{61}C_{65}(16)$
176			239	230	1.88	0.74	1.23	0.34	$\tau H_{23}C_{22}C_{19}C_{16}(25)$
177			229	220	0.42	0.17	3.93	1.10	$\beta C_{22}C_{19}C_{16}(20)$
178		207	217	208	0.42	0.17	1.62	0.45	$\beta H_{23}C_{22}C_{19}C_{16}(11)$
179			203	195	0.70	0.28	7.00	1.95	$\beta N_{27}C_{32}S_{31}$ (12)
180			183	176	0.59	0.23	1.77	0.49	$\beta C_{38}C_{36}C_1$ (14)+$\beta N_{48}C_{46}S_5$ (11)
181		155	161	155	8.17	3.23	5.69	1.59	$\beta C_{60}C_{58}N_{28}$ (10)+$\beta C_{58}N_{28}C_{32}$ (15)
182			142	136	1.82	0.72	2.33	0.65	$\tau C_{32}N_{27}N_{26}C_3(18)+\tau C_1C_2C_3N_{26}(12)$
183			121	116	2.33	0.92	0.37	0.10	$\tau N_{28}C_{32}N_{27}N_{26}(14)$
184			116	111	0.29	0.11	1.53	0.43	$\beta C_3C_2C_{11}$ (10)+$\tau N_{28}C_{32}N_{27}N_{26}(11)$
185			95	91	0.21	0.08	0.90	0.25	$\tau C_{22}C_{19}C_{16}C_{14}(38)+\tau C_{19}C_{16}C_{14}C_{11}(31)$
186			86	83	0.08	0.03	2.52	0.70	$\tau C_1N_9C_5C_{46}(16)+\tau C_5N_9C_1C_{36}(16)$
187			79	76	0.26	0.10	1.01	0.28	$\tau H_{22}C_{19}C_{16}C_{14}(17)$
188		71	73	70	0.10	0.04	2.02	0.56	$\Gamma C_1C_{36}C_{38}C_{37}(15)+\tau C_5N_9C_1C_{36}(10)$
189			51	49	0.10	0.04	9.10	2.54	$\beta C_{46}C_5N_9$ (11)+$\tau C_{38}C_{36}C_1N_9(18)$
190			49	47	0.10	0.04	6.54	1.82	$\tau C_{38}C_{36}C_1N_9(42)+\tau C_{58}N_{28}C_{32}N_{27}(11)+\tau C_1N_9C_5C_{46}(11)$
191			43	41	0.03	0.01	1.76	0.49	$\beta C_{36}C_1N_9$ (15)+$\tau C_{38}C_{36}C_1N_9(19)+\tau C_{58}N_{28}C_{32}N_{27}(10)$
192			36	35	0.52	0.21	0.61	0.17	$\beta C_{32}N_{27}N_{26}$ (11)+$\beta N_{27}N_{26}C_3$ (11)+$\tau C_{58}N_{28}C_{32}N_{27}(10)$
193			32	31	0.77	0.30	4.66	1.30	$\tau C_{48}N_{46}C_5N_9(16)+\tau C_{32}N_{28}C_{58}C_{60}(16)+\tau C_{32}N_{27}N_{26}C_3(12)$
194			28	27	0.40	0.16	9.35	2.61	$\tau C_{48}C_{46}C_5N_9(55)+\tau C_{16}C_{14}C_{11}C_2(16)$
195			25	24	0.36	0.14	2.05	0.57	$\beta C_{58}N_{28}C_{32}$ (10)+$\tau C_{32}N_{28}C_{58}C_{60}(13)+\tau C_{16}C_{14}C_{11}C_2(45)$
196			19	18	0.44	0.18	1.74	0.48	$\tau C_{48}C_{46}C_5N_9(10)+\tau C_{32}N_{27}N_{26}C_3(22)$
197			18	17	2.10	0.83	4.53	1.26	$\tau C_{28}C_{32}N_{27}N_{26}(13)+\tau C_2C_3N_{26}N_{27}(13)+\Gamma C_1C_2N_9C_3(10)$
198			14	13	0.0318	0.0126	2.0202	0.5634	$\tau C_{32}N_{27}N_{26}C_3(13)+\tau C_{58}N_{28}C_{32}N_{27}(15)+\tau C_1C_2C_3N_{26}(20)$

ν: Stretching, β: in-plane-bending, Γ: out-of-plane bending, τ: Torsion, vw: very week, w: week, m: medium, s: strong, vs: very strong,

[a] Scaling factor: 0.9608,

[b] Relative IR absorption intensities normalized with highest peak absorption equal to 100,

[c] Relative Raman intensities calculated and normalized to 100,

[d] Total energy distribution calculated at B3LYP/6-311++G(d,p) level.

Table 3. The NLO measurements of 3-PDPPPHC.

Parameter	Hyperpolarizability	Parameter	Polarizability
β_{xxx}	27.0596	α_{xx}	-195.3236
β_{yyy}	60.4279	α_{yy}	-210.9731
β_{zzz}	-2.5280	α_{zz}	-206.3976
β_{xyy}	-71.6706	α_{xy}	12.9496
β_{xxy}	20.4510	α_{xz}	3.6875
β_{xxz}	-6.5713	α_{yz}	-7.3381
β_{xzz}	3.7648	α_{o} (esu)	0.32671 $X10^{-30}$ esu
β_{yzz}	17.0146		
β_{yyz}	39.1729		
β_{xyz}	-24.8329		
β_{0} (esu)	9.52518 $X10^{-30}$ esu		

Standard value for urea (**μ**=1.3732 Debye, β_0=0.3728x10^{-30}esu): **esu**-electrostatic unit

Table 4. The NBO analysis of 3-PDPPPHC.

Type	Donor NBO (i)	ED/e	Acceptor NBO (j)	ED/e	$E^{(2)}$ KJ/mol	E(j)-E(i) a.u.	F(i, j) a.u.
π -π*	BD (2) C37 - C39	1.66588	BD*(2) C36 - C38	0.35003	86.94	0.28	0.069
π -π*	BD (2) C41 - C43	1.66448	BD*(2) C36 - C38	0.35003	83.97	0.28	0.067
			BD*(2) C51 - C53	0.33318	87.11	0.28	0.068
π -π*	BD (2) C47 - C49	1.66656	BD*(2) C46 - C48	0.34829	87.03	0.28	0.069
			BD*(2) C51 - C53	0.33318	84.39	0.28	0.067
π -π*	BD (2) C51 - C53	1.66295	BD*(2) C46 - C48	0.34829	83.72	0.28	0.067
			BD*(2) C47 - C49	0.32671	85.44	0.28	0.068
π -π*	BD (2) C58 - C59	1.65941	BD*(2) C61 - C65	0.34741	88.7	0.29	0.07
n -σ*	LP (1) N26	1.91379	BD*(1) C2 - C3	0.05081	63.14	0.75	0.096
n -π*	LP (1) N27	1.67942	BD*(2) C3 - N26	0.17095	112.93	0.31	0.084
			BD*(1) S31 - C32	0.44774	238.28	0.23	0.106
n -σ*	LP (1) N28	1.68391	BD*(1) S31 - C32	0.44774	224.26	0.22	0.1
n -σ*	LP (2) S31	1.86707	BD*(1) N27 - C32	0.0695	55.48	0.59	0.08
π*-π*	BD*(2) C58 - C59	0.40213	BD*(2) C61 - C65	0.34741	1285.12	0.01	0.081

Table 5. The Physico-Chemical properties of 3-PDPPPHC.

Parameters	Values
HOMO	-5.249 eV
LUMO	-0.951 eV
Energy gap	4.298 eV
HOMO-1	-5.527 eV
LUMO+1	-0.368 eV
Ionization potential (IP)	5.249 eV
Electron affinity (EA)	0.951 eV
Electrophilicity Index (ω)	1.118
Chemical Potential (μ)	3.101
Electro negativity (χ)	-3.101
Hardness (η)	-4.298

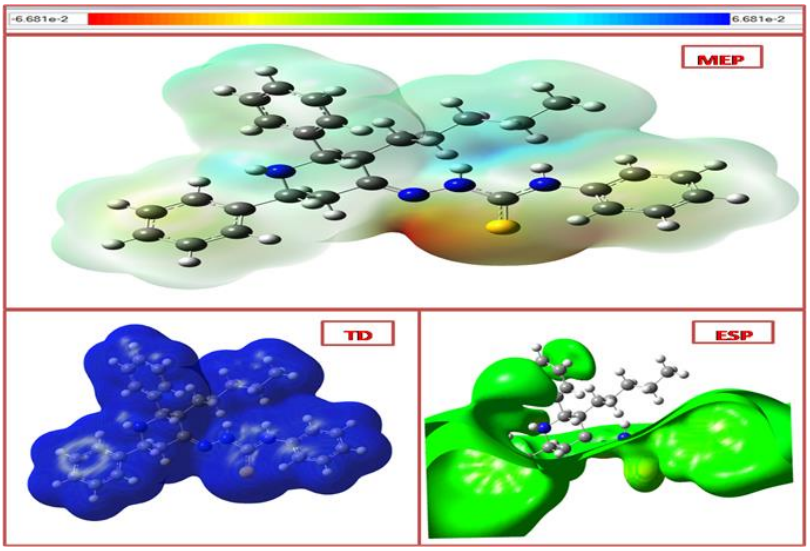

Figure 6. Electrostatic potential (ESP), total density (TD) and the molecular electrostatic potential (MEP) map in gas phase of 3-PDPPPHC.

3.8. Mulliken atomic charges.

Mulliken atomic charge calculation has an important role in applying quantum chemical calculation to the molecular system since atomic charges affect the dipole moment, molecular polarizability, electronic structure, and many more molecular systems properties. In the present study, the Mulliken charges were calculated by DFT/B3LYP/6-311++G(d,p) basis set. The calculated Mulliken charge values are listed in Table 6 and are plotted in Fig. 7. The C22/C32 atoms have the highest negative/positive charges, respectively, among the other atoms in the 3-PDPPPHC molecule due to the resonance. The Nitrogen and sulfur atoms have negative charges and all hydrogen atoms having net positive charges in the present system.

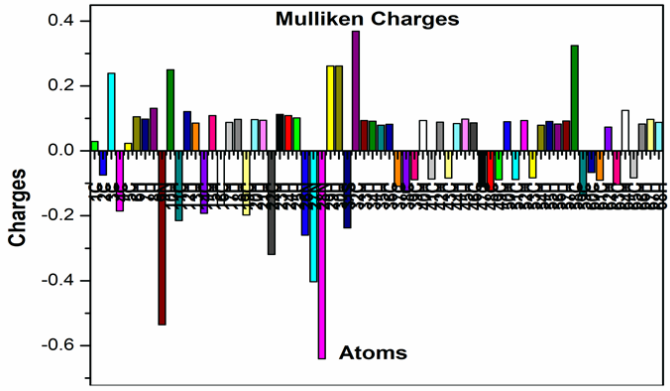

Figure 7. The Mulliken atomic charges of 3-PDPPPHC.

Table 6. The Mulliken atomic charges of 3-PDPPPHC.

Atom	Charges	Atom	Charges	Atom	Charges
1C	0.02905	24H	0.10917	47C	-0.1103
2C	-0.0741	25H	0.10188	48C	-0.1221
3C	0.23892	26N	-0.2598	49C	-0.0891
4C	-0.1852	27N	-0.403	50H	0.08993
5C	0.02328	28N	-0.6404	51C	-0.0878
6H	0.10552	29H	0.26156	52H	0.0935
7H	0.09778	30H	0.26132	53C	-0.0834
8H	0.13144	31S	-0.2371	54H	0.07883
9N	-0.5359	32C	0.36851	55H	0.09093
10H	0.2498	33H	0.09341	56H	0.08292
11C	-0.2148	34H	0.09128	57H	0.09221
12H	0.12148	35H	0.07892	58C	0.32464
13H	0.08562	36C	0.08201	59C	-0.1392
14C	-0.1921	37C	-0.109	60C	-0.0665
15H	0.109	38C	-0.1287	61C	-0.09
16C	-0.1669	39C	-0.0888	62H	0.07336
17H	0.08814	40H	0.09359	63C	-0.1038
18H	0.09697	41C	-0.0866	64H	0.12507
19C	-0.1976	42H	0.08828	65C	-0.0832
20H	0.09682	43C	-0.0836	66H	0.08265
21H	0.09424	44H	0.08443	67H	0.0974
22C	-0.3193	45H	0.09818	68H	0.0875
23H	0.1123	46C	0.08639		

3.9. Thermodynamic properties.

Based on the vibrational analysis carried out at the B3LYP/6-311++G(d,p) level, the standard statistical thermodynamic functions such as heat capacity (Cp), entropy (S), and enthalpy changes (ΔH) are calculated for the present molecule. The values are listed in Table 7. It can be observed that these thermodynamic functions are increasing with temperature. The obvious reason for this almost linear increase is the increase in the molecule's internal energy

in accordance with the kinetic theory of gases [55]. The correlation equations between thermodynamic functions and temperatures were fitted by quadratic formula. The corresponding fitting factors (R^2) for these thermodynamic properties are found to be 0.99878, 0.99998, and 0.99952, respectively. The corresponding correlation graphs are shown in Fig. 8.

$$C^0_{p.m} = -0.77064 + 0.49207\ T - 1.90845\ X\ 10^{-4}\ T^2\ (R^2 = 0.99878)$$

$$S^0_m = 78.34872 + 0.48239\ T - 8.82755\ X\ 10^{-5}\ T^2\ (R^2 = 0.99998)$$

$$H^0_m = -4.65157 + 0.04631\ T + 1.42948\ X\ 10^{-4}\ T^2\ (R^2 = 0.99952)$$

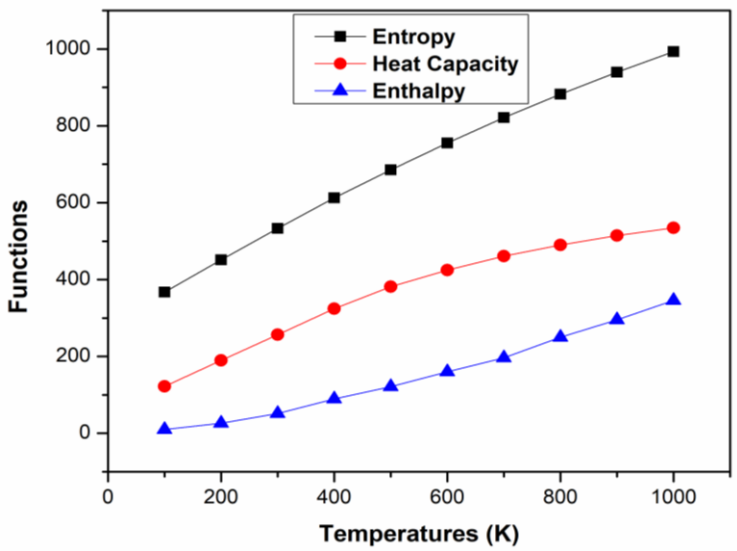

Figure 8. The thermodynamic properties at different temperatures of 3-PDPPPHC.

Table 7. The Thermodynamic properties at different temperatures of 3-PDPPPHC.

T	S(J/mol.K)	Cp(J/mol.K)	ddH(kJ/mol)
100	367.21	122.43	9.87
200	451.17	189.58	26.22
300	533.29	256.41	51.47
400	612.32	324.51	89.12
500	685.21	381.24	121.18
600	755.02	424.81	160.37
700	821.71	461.23	196.68
800	882.51	490.24	249.68
900	939.72	514.31	295.45
1000	992.91	534.19	345.72

3.10. Molecular docking studies.

The dock, glide energy, and hydrogen bonding interactions of the title compound and co-crystallized ligand are given in Table 8. A view of the X-ray crystal structure of the title compound in the Beta-lactamase Receptor active site showing the key hydrogen contacts between inhibitor and enzyme is depicted in Fig. 9. The co-crystallized ligand in the Beta-lactamase Receptor active site showing the key hydrogen contacts between inhibitor and enzyme is depicted in Fig. 10. The surface diagram showing the title compound docked at Beta-lactamase Receptor's active site is depicted in Fig. 11.

X-ray crystal structures confirmed the expected binding mode. Considering binding orientation and electronic properties enabled optimization to Piperidone as a more potent second-generation lead.

The title compound is shown to be an effective inhibitor. The amide group in the GLY286 interacts with the carbonyl group's oxygen atom at a distance of 2.8 & 3.0 Å. The co-crystallized ligand also docked well, and it shows better interactions with residues GLY and

THR, respectively. The results show that the title compound has better binding energy, and the co-crystallized ligand has comparable interactions.

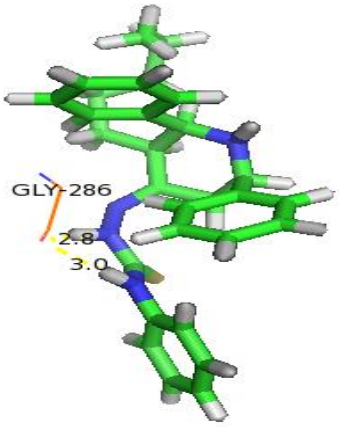

Figure 9. The title compound in the Beta-lactamase Receptor active site showing the key hydrogen contacts between Piperidone inhibitor and enzyme.

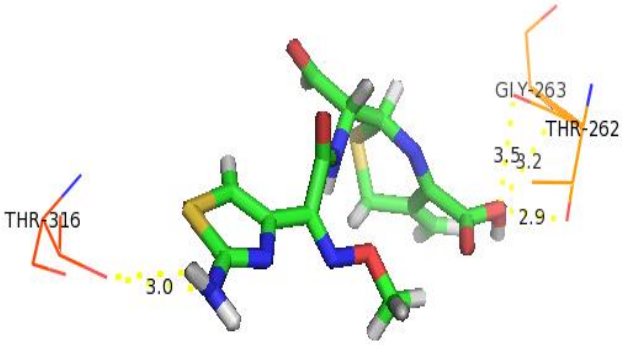

Figure 10. The co-crystallized ligand (dexamethasone) in the Beta-lactamase Receptor active site showing the key hydrogen contacts between inhibitor and enzyme.

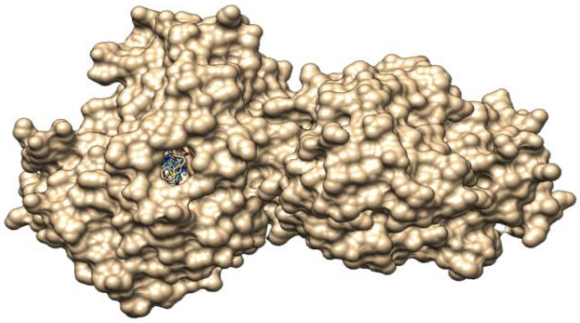

Figure 11. Surface diagram showing the Piperidone docked at the active site of beta-lactamase Receptor.

Table 8. Hydrogen bond interactions of Piperidone with amino acids at the active site of Beta-lactamase Receptor.

Compound	Docking Score	Hydrogen Bonding Interactions		
		Donor	Acceptor	Distance (Å)
Piperidone	-6.1	N-H N-H	O[GLY-286	**2.8** **3.0**
		O-H[THR263]	O*	3.2 2.9
Co-Crystal	-5.4	N-H[THR316]	O*	3.0
		O-H[GLY263]	O*	3.5

* Ligand

Table 9. Prediction of ADME/Tox.

ID	Value
BBB	7.65083
Buffer_solubility_mg_L	1.63674
Caco2	36.2157
CYP_3A4_substrate	Substrate
HIA	95.447711
MDCK	18.6595
Plasma_Protein_Binding	87.031791
Water_solubility_mg_L	0.000931924
Skin_Permeability	-1.79587
SKlogD_value	5.71791
SKlogP_value	7.06189
SKlogS_buffer	-5.45874
SKlogS_pure	-8.70334

BBB-blood-brain barrier penetration

HIA-Human intestinal absorption

3.11. ADME analysis.

In drug discovery, physicochemical properties were seen to find the vital properties affecting the biological functions (ADME). In this analysis, some important physicochemical properties were given in Table 9. The concept of absorption, distribution, metabolism, and excretion (ADME) shows small molecules' toxicity levels [56]. Drug discovery in silico method has been used to predict pharmacokinetic properties for instant ADMET accurately.

4. Conclusions

The FT-IR and FT-Raman spectra of 3-PDPPPHC have been recorded and analyzed for the first time. The detailed interpretations of the vibrational spectra have been carried out. The optimized geometrical parameters were calculated and compared with a structurally related molecule, which shows the chair conformation. The calculated and experimental results of all the fundamental vibrational modes of 3-PDPPPHC are examined with TED contribution. Besides, the first hyperpolarizability value of the molecule is high, i.e., twenty-six times greater than that of urea; hence, the molecule's NLO activity will also be proportionately high. The NBO result reflects more hyperconjugative interaction energy during π-electron transfer within π-π* interaction, and it leads that the molecule becomes more active. The lowering of the HOMO-LUMO energy gap value has a substantial influence on the ICT and bioactivity of the molecule. The Mulliken atomic charges were calculated and analyzed. The MEP surface predicts the nucleophilic and electrophilic reaction sites of the molecule. The thermodynamic properties such as heat capacity, entropy, and enthalpy at different temperatures were also calculated. Molecular docking results show that the title compound having better binding energy, and the co-crystallized ligand has comparable interactions.

Funding

This research received no external funding.

Acknowledgments

This research has no acknowledgment.

Conflicts of Interest

The authors declare no conflict of interest.

References

1. Khan, S.A.; Kumar, P.; Joshi, R.; Iqbal, P.F.; Saleem, K. Synthesis and in vitro antibacterial activity of new steroidal thiosemicarbazone derivatives. *European Journal of Medicinal Chemistry* **2008,** *43,* 2029–2034, http://dx.doi.org/10.1016/j.ejmech.2007.12.004.
2. De Araújo Neto, L.N.; de Lima M do, C.A.; de Oliveira, J.F.; de Souza, E.R.; Feitosa Machado, S.E.; de Souza Lima, G.M. Thiophene-thiosemicarbazone derivative (L10) exerts antifungal activity mediated by oxidative stress and apoptosis in C. albicans. *Chemico-Biological Interactions* **2020,** *320,* http://dx.doi.org/10.1016/j.cbi.2020.109028.
3. De Oliveira, R.B.; de Souza-Fagundes, E.M.; Soares, R.P.P.; Andrade, A.A.; Krettli, A.U.; Zani, C.L. Synthesis and antimalarial activity of semicarbazone and thiosemicarbazone derivatives. *European Journal of Medicinal Chemistry* **2008,** *43,* 1983–1988, http://dx.doi.org/10.1016/j.ejmech.2007.11.012.
4. Matsa, R.; Makam, P.; Kaushik, M.; Hoti, S.L.; Kannan, T. Thiosemicarbazone derivatives: Design, synthesis and in vitro antimalarial activity studies. *European Journal of Pharmaceutical Sciences* **2019,** *137,* http://dx.doi.org/10.1016/j.ejps.2019.104986.
5. Ameryckx, A.; Pochet, L.; Wang, G.; Yildiz, E.; Saadi, B.E.; Wouters, J. Pharmacomodulations of the benzoyl-thiosemicarbazide scaffold reveal antimicrobial agents targeting d-alanyl-d-alanine ligase in bacterio. *European Journal of Medicinal Chemistry* **2020,** *200,* http://dx.doi.org/10.1016/j.ejmech.2020.112444.
6. Zhang, X.; Qi, F.; Wang, S.; Song, J.; Huang, J. Synthesis, structure, in silico ADME evaluation and in vitro antioxidant of (E)-N-(4-ethylphenyl)-2-(isomeric methylbenzylidene) thiosemicarbazone derivatives. *Journal of Molecular Structure* **2020,** *1199,* http://dx.doi.org/10.1016/j.molstruc.2019.126972.
7. Afrasiabi, Z.; Sinn, E.; Kulkarni, P.P.; Ambike, V.; Padhye, S.; Deobagakar, D. Synthesis and characterization of copper(II) complexes of 4-alkyl/aryl-1,2-naphthoquinones thiosemicarbazones derivatives as potent DNA cleaving agents. *Inorganica Chimica Acta* **2005,** *358,* 2023–2030, http://dx.doi.org/10.1016/j.ica.2004.12.042.
8. Song, J.; Pan, R.; Li, G.; Su, W.; Song, X.; Li, J. Synthesis and anticancer activities of thiosemicarbazones derivatives of thiochromanones and related scaffolds. *Medicinal Chemistry Research* **2020,** *5,* 630–642, http://dx.doi.org/10.1007/s00044-020-02503-w.
9. He, Z.; Qiao, H.; Yang, F.; Zhou, W.; Gong, Y.; Zhang, X. Novel thiosemicarbazone derivatives containing indole fragment as potent and selective anticancer agent. *European Journal of Medicinal Chemistry* **2019,** *184,* http://dx.doi.org/10.1016/j.ejmech.2019.111764.
10. Taroua, M.; Ribuot, C.; Péra, M.; Taillandier, G.; Fatome, M.; Laval, J. New α, β and y semicarbazone and thiosemicarbazone 1,3-dithiolanes as radioprotectors. Anticonvulsant activity. *European Journal of Medicinal Chemistry* **1996,** *31,* 589–95, http://dx.doi.org/10.1016/0223-5234(96)89554-7.
11. Trotsko, N.; Golus, J.; Kazimierczak, P.; Paneth, A.; Przekora, A.; Ginalska, G. Design, synthesis and antimycobacterial activity of thiazolidine-2,4-dione-based thiosemicarbazone derivatives. *Bioorganic Chemistry* **2020,** *97,* http://dx.doi.org/10.1016/j.bioorg.2020.103676.
12. Ribeiro, A.G.; Almeida, S.M.V.; de Oliveira, J.F.; de Souza T.R.C.; dos Santos, K.L.; Albuquerque, A.P. Novel 4-quinoline-thiosemicarbazone derivatives: Synthesis, antiproliferative activity, in vitro and in silico biomacromolecule interaction studies and topoisomerase inhibition. *European Journal of Medicinal Chemistry* **2019,** *182,* http://dx.doi.org/10.1016/j.ejmech.2019.111592.
13. Da Silva, P.R.; de Oliveira, J.F.; da Silva, A.L.; Queiroz, C.M.; Feitosa, A.P.S.; Duarte D.M.F.A. Novel indol-3-yl-thiosemicarbazone derivatives: Obtaining, evaluation of in vitro leishmanicidal activity and ultrastructural studies. *Chemico-Biological Interactions* **2020,** *315,* http://dx.doi.org/10.1016/j.cbi.2019.108899.
14. Sagnou, M.; Mavroidi, B.; Kaminari, A.; Boukos, N.; Pelecanou, M. Novel Isatin Thiosemicarbazone Derivatives as Potent Inhibitors of β-Amyloid Peptide Aggregation and Toxicity. *ACS Chemical Neuroscience* **2020,** *29, 11,* 2266–2276, http://dx.doi.org/10.1021/acschemneuro.0c00208.
15. Hussein, M.A.; Iqbal, M.A.; Umar, M.I.; Haque, R.A.; Guan, T.S. Synthesis, structural elucidation and cytotoxicity of new thiosemicarbazone derivatives. *Arabian Journal of Chemistry* **2019,** *12,* 3183–3192, http://dx.doi.org/10.1016/j.arabjc.2015.08.013.
16. Da Silva Filho, F.A.; de Freitas Souza, T.; Ribeiro, A.G.; Alves, J.E.F.; de Oliveira, J.F.; de Lima Souza, T.R.C. Topoisomerase inhibition and albumin interaction studies of acridine-thiosemicarbazone derivatives. *International Journal of Biological Macromolecules* **2019,** *138,* 582–589, http://dx.doi.org/10.1016/j.ijbiomac.2019.07.097.
17. Bahojb Noruzi, E.; Shaabani, B.; Geremia, S.; Hickey, N.; Nitti, P.; Kafil, H.S. Synthesis, Crystal Structure, and Biological Activity of a Multidentate Calix[4]arene Ligand Doubly

Functionalized by 2-Hydroxybenzeledene-Thiosemicarbazone. *Molecules* **2020,** *16*, http://dx.doi.org/10.3390/molecules25020370.
18. Siddiqui, E.J.; Azad, I.; Khan, A.R.; Khan, T. Thiosemicarbazone Complexes as Versatile Medicinal Chemistry Agents: A Review. *Journal of Drug Delivery and Therapeutics* **2019,** *9*, 689-703.
19. Mendes, E.P.; Goulart, C.M.; Chaves, O.A.; Faiões, V.d.S.; Canto-Carvalho, M.M.; Machado, G.C.; Torres-Santos, E.C.; Echevarria, A.Evaluation of Novel Chalcone-Thiosemicarbazones Derivatives as Potential Anti-Leishmania amazonensis Agents and Its HSA Binding Studies. *Biomolecules* **2019,** *23*, http://dx.doi.org/10.3390/biom9110643.
20. Pham, V.H.; Phan, T.P.D.; Phan, D.C.; Vu, B.D. Synthesis and Bioactivity of Thiosemicarbazones Containing Adamantane Skeletons. *Molecules* **2020,** *13*, http://dx.doi.org/10.3390/molecules25020324.
21. Ishaq, M.; Taslimi, P.; Shafiq, Z.; Khan, S.; Ekhteiari Salmas, R.; Zangeneh, M.M. Synthesis, bioactivity and binding energy calculations of novel 3-ethoxysalicylaldehyde based thiosemicarbazone derivatives. *Bioorganic Chemistry* **2020,** *100*, http://dx.doi.org/10.1016/j.bioorg.2020.103924.
22. Klayman, D.L.; Scovill, J.P.; Bartosevich, J.F.; Mason, C.J. 2-Acetylpyridine thiosemicarbazones. 2. N4,N4-Disubstituted derivatives as potential antimalarial agents. *Journal of Medicinal Chemistry* **1979,** *22*, 1367–1373, http://dx.doi.org/10.1021/jm00197a017.
23. Pandeya, S.N.; Ponnilavarasan, I.; Pandey, A.; Lakhan, R.; Stables, J.P. Evaluation of p-nitrophenyl substituted semicarbazones for anticonvulsant properties. *Die Pharmazie* **1999**, *54*, 923-925.
24. Pandeya, S.N.; Manjula, H.; Stables, J.P. Design of semicarbazones and their bio-isosteric analogues as potential anticonvulsants. *Pharmazie* **2001,** *56*, 121-124, http://dx.doi.org/10.1002/chin.200118081.
25. Bharti, N.; Husain, K.; Gonzalez Garza, M.; Cruz-Vega, D.E.; Castro-Garza, J.; Mata-Cardenas, B.D. Synthesis and in vitro antiprotozoal activity of 5-nitrothiophene-2-carboxaldehyde thiosemicarbazone derivatives. *Bioorganic & Medicinal Chemistry Letters* **2002,** *12*, 3475–3478, http://dx.doi.org/10.1016/s0960-894x(02)00703-5.
26. Fahmi, N.; Singh, R.V. Spectroscopic, antifungal, and antibacterial studies of some manganese heterochelates. *Journal of the Indian Chemical Society* **1996,** *73*, 257-259, https://doi.org/10.1002/chin.199740303.
27. Anitha, L.; Saritha, S.R.; Layana, S.R.; Nair Lakshmi, C.S.; Hubert Joe, I.; Sudarsanakumar, M.R. Structural studies of 3-[(E)-[(2E)-2-methyl-3-phenylprop-2-en-1-ylidene] amino]-1-phenylthiourea: Combined experimental and computational studies. *Journal of Molecular Structure* **2019,** *1191*, 206–217, http://dx.doi.org/10.1016/j.molstruc.2019.04.062.
28. Basri, R.; Khalid, M.; Shafiq, Z.; Tahir, M.S.; Khan, M.U.; Tahir, M.N. Exploration of Chromone-Based Thiosemicarbazone Derivatives: SC-XRD/DFT, Spectral (IR, UV–Vis) Characterization, and Quantum Chemical Analysis. *ACS Omega* **2020,** *10*, 30176–30188, http://dx.doi.org/10.1021/acsomega.0c04653.
29. Zhang, H.H.; Qin, C.K.; Chen, Y.; Zhang, Z. Inhibition behaviour of mild steel by three new benzaldehyde thiosemicarbazone derivatives in 0.5M H_2SO_4: experimental and computational study. *Royal Society Open Science* **2019,** *6*, http://dx.doi.org/10.1098/rsos.190192.
30. Vijayan, N.; Ramesh Babu, R.; Gopalakrishnan, R.; Dhanuskodi, S.; Ramasamy, P. Growth and characterization of organic NLO crystals of semicarbazone of acetophenone. *Journal of Crystal Growth* **2001,** *233*, 863–867, http://dx.doi.org/10.1016/s0022-0248(01)01628-1.
31. Ramesh Babu, R.; Vijayan, N.; Gopalakrishnan, R.; Ramasamy, P. Growth and characterisation of benzaldehyde semicarbazone (BSC) single crystals. *Journal of Crystal Growth***2002,***240*, 545–548, http://dx.doi.org/10.1016/s0022-0248(02)01075-8.
32. Sethuraman, K.; Ramesh Babu, R.; Vijayan, N.; Gopalakrishnan, R.; Ramasamy, P. Synthesis, growth of organic non-linear optical crystal: Semicarbazone of 2-amino-5-chloro-benzophenone (S2A5CB) and its characterisation. *Journal of Crystal Growth* **2006,** *290*, 539–543, http://dx.doi.org/10.1016/j.jcrysgro.2006.01.038.
33. Sebastian, S.; Sundaraganesan, N.; Manoharan, S. Molecular structure, spectroscopic studies and first-order molecular hyperpolarizabilities of ferulic acid by density functional study. *Spectrochimica Acta Part A: Molecular and Biomolecular Spectroscopy* **2009,** *74*, 312–323, http://dx.doi.org/10.1016/j.saa.2009.06.011.
34. Abraham, J.P.; Joe, I.H.; George, V.; Nielsen, O.F.; Jayakumar, V.S. Vibrational spectroscopic studies on the natural product, columbianadin. *Spectrochimica Acta Part A: Molecular and Biomolecular Spectroscopy* **2003,** *59*, 193–199, http://dx.doi.org/10.1016/s1386-1425(02)00148-8.
35. Binoy, J.; Abraham, J.P.; Joe, I.H.; George, V.; Jayakumar, V.S.; Aubard, J. Near-infrared Fourier transform Raman, surface-enhanced Raman scattering and Fourier transform infrared spectra andab initio calculations of the natural product nodakenetin angelate. *Journal of Raman Spectroscopy* **2005,** *36*, 63–72, http://dx.doi.org/10.1002/jrs.1272.
36. Arockia Doss, M.; Savithiri, S.; Rajarajan, G.; Thanikachalam, V. Synthesis, spectral, stereochemical and biological evaluation of (E)-2-(3-pentyl-2,6-diarylpiperidin-4-ylidene)-N-phenylhydrazinecarbothioamide derivatives. *Phosphorus, Sulfur, and Silicon and the Related Elements* **2017,** *11*, 1264–1270, http://dx.doi.org/10.1080/10426507.2017.1315580.

37. Frisch, M.J.; Trucks, G.W.; Schlegel, H.B.; Scuseria, G.E.; Robb, M.A.; Cheeseman, J.R.; Scalmani, G.; Barone, V.; Mennucci, B.; Petersson, G.; Nakatsuji, H. *Gaussian 09, Revision d. 01, Gaussian. Inc.*, Wallingford CT, 201. **2009**.
38. Jamroz, M.H. *Vibrational Energy Distribution Analysis*.VEDA 4 Computer Program, Poland, **2004**.
39. Glendening, E.D.; Reed, A.E.; Carpenter, J.E.; Weinhold, F. *NBO Version 3.1*. TCI, University of Wisconsin, Madison, **1998**.
40. O'boyle, N.M.; Tenderholt, A.L.; Langner, K.M. cclib: A library for package-independent computational chemistry algorithms. *Journal of Computational Chemistry* **2008,** *29*, 839–845, http://dx.doi.org/10.1002/jcc.20823.
41. Thomas, V.L.; McReynolds, A.C.; Shoichet, B.K. Structural Bases for Stability–Function Tradeoffs in Antibiotic Resistance. *Journal of Molecular Biology* **2010,** *396*, 47–59, http://dx.doi.org/10.1016/j.jmb.2009.11.005.
42. Bikadi, Z.; Hazai, E. Application of the PM6 semi-empirical method to modeling proteins enhances docking accuracy of AutoDock. *Journal of Cheminformatics* **2009,** *11*, http://dx.doi.org/10.1186/1758-2946-1-15.
43. Morris, G.M.; Goodsell, D.S.; Robert, S.; Halliday, Ruth Huey, W.E.; Hart, R.K.; Belew, A.J.; Olsonet. Automated docking using a Lamarckian genetic algorithm and an empirical binding free energy function. *Journal. of Computational Chemistry* **1998,** *19*, 1639-1662, https://doi.org/10.1002/(SICI)1096-987X(19981115)19:14<1639.
44. Savithiri, S.; Arockia doss, M.; Rajarajan, G.; Thanikachalam, V.; Bharanidharan, S.; Saleem, H. Spectroscopic (FT-IR, FT-Raman) and quantum mechanical studies of 3t-pentyl-2r,6c-diphenylpiperidin-4-one thiosemicarbazone. *Spectrochimica Acta Part A: Molecular and Biomolecular Spectroscopy* **2015,** *136*, 782–92, http://dx.doi.org/10.1016/j.saa.2014.09.095.
45. Rauhut, G.; Pulay, P. Transferable Scaling Factors for Density Functional Derived Vibrational Force Fields. *The Journal of Physical Chemistry* **1995,** *99*, 3093–3100, http://dx.doi.org/10.1021/j100010a019.
46. Dhandapani, A.; Manivarman, S.; Subashchandrabose, S.; Saleem, H. Molecular structure and vibrational analysis on (E)-1-(3-methyl-2,6-diphenyl piperidin-4-ylidene) semicarbazide. *Journal of Molecular Structure* **2014,** *1058*, 41–50, http://dx.doi.org/10.1016/j.molstruc.2013.09.052.
47. Krishnakumar, V.; Balachandran, V. Structures and vibrational frequencies of 2-hydroxy-3-methoxy-5-nitrobenzaldehyde and 2-methoxy-1-naphthaldehyde based on density functional theory calculations. *Spectrochimica Acta Part A: Molecular and Biomolecular Spectroscopy* **2006,** *63*, 464–476, http://dx.doi.org/10.1016/j.saa.2005.05.032.
48. Reed, A.E.; Curtiss, LA.; Weinhold, F. Intermolecular interactions from a natural bond orbital, donor-acceptor viewpoint. *Chemical Reviews* **1988,** *88*, 899–926, http://dx.doi.org/10.1021/cr00088a005.
49. Silverstein, R.M.; Webster, F.X. *Spectroscopic Identification of Organic Compounds*.7th ed., Wiley, New York, **2005**.
50. Singh, D.K.; Srivastava, S.K.; Ojha, A.K.; Asthana, B.P. Vibrational study of thiophene and its solvation in two polar solvents, DMSO and methanol by Raman spectroscopy combined with ab initio and DFT calculations. *Journal of Molecular Structure* **2008,** *892*, 384–391, http://dx.doi.org/10.1016/j.molstruc.2008.06.008.
51. Gussoni, M.; Castiglioni, C.; Ramos, M.N.; Rui, M.; Zerbi, G. Infrared intensities: from intensity parameters to an overall understanding of the spectrum. *Journal of Molecular Structure* **1990,** *224*, 445–470, http://dx.doi.org/10.1016/0022-2860(90)87033-t.
52. Geskin, V.M.; Lambert, C.; Brédas, J.L. Origin of High Second- and Third-Order Nonlinear Optical Response in Ammonio/Borato Diphenylpolyene Zwitterions: the Remarkable Role of Polarized Aromatic Groups. *Journal of the American Chemical Society* **2003,** *125*, 15651–15658, http://dx.doi.org/10.1021/ja035862p.
53. James, C.; Raj, A.A.; Reghunathan, R.; Jayakumar, V.S.; Joe, I.H. Structural conformation and vibrational spectroscopic studies of 2,6-bis(p-N,N-dimethyl benzylidene)cyclohexanone using density functional theory. *Journal of Raman Spectroscopy* **2006,** *37*, 1381–1392, http://dx.doi.org/10.1002/jrs.1554.
54. Murray, J.S.; Sen, K. *Molecular Electrostatic Potentials*. Concepts and 399 Applications, Elsevier, Amsterdam, **1996**.
55. Ott, J.B.; Boerio-Goates, J. Statistical Thermodynamics. *Chemical Thermodynamics: Principles and Applications* **2000,** 497–592, http://dx.doi.org/10.1016/b978-012530990-5/50011-0.
56. Pajouhesh, H.; Lenz, G.R. Medicinal chemical properties of successful central nervous system drugs. *NeuroRX* **2005,** *2*, 541–553, http://dx.doi.org/10.1602/neurorx.2.4.541.